Scilight

Physics and the Cosmos
https://www.sciltp.com/journals/pac

Review

Check for updates

Molecular Clouds as Multi-Messenger Sources: Cosmic Rays, Gamma Rays, and Neutrinos from Galactic Hadronic Interactions

Luiz Augusto Stuani Pereira [1,2]

[1] Instituto de Física da Universidade de São Paulo (IFUSP), São Paulo 05508-090, Brazil; luizstuani@uaf.ufcg.edu.br
[2] Unidade Acadêmica de Física da Universidade Federal de Campina Grande (UAF-UFCG), Campina Grande 58429-900, Brazil

How To Cite: Pereira, L.A.S. Molecular Clouds as Multi-Messenger Sources: Cosmic Rays, Gamma Rays, and Neutrinos from Galactic Hadronic Interactions. *Physics and the Cosmos* **2026**, *1*(1), 7. https://doi.org/10.53941/pac.2026.100007

Received: 16 March 2026
Revised: 31 March 2026
Accepted: 2 April 2026
Published: 30 April 2026

Abstract: Molecular clouds are among the most promising multimessenger sources in the Galaxy. When illuminated by cosmic rays accelerated in nearby sources such as supernova remnants, young massive stellar clusters, or pulsar wind nebulae, these dense gas reservoirs can act as hadronic interaction targets, ranging from optically thin emitters to partially calorimetric systems depending on their density, size, and the transport properties of cosmic rays within them, converting a fraction of the cosmic-ray energy into gamma rays and neutrinos through proton-proton interactions and the subsequent decay of charged and neutral pions. In this review, we discuss the physical mechanisms underlying these interactions, including the pion-decay spectral signature, the nuclear enhancement factor, and the energy-dependent diffusion of cosmic rays within and around molecular clouds. We survey the observational landscape from GeV to ultra-high energies: the Fermi-LAT detection of the pion-decay spectral break in supernova remnant-cloud systems, the H.E.S.S. measurement of a $1/r$ cosmic-ray density profile in the Central Molecular Zone, establishing the Galactic center as a PeVatron candidate, and the LHAASO observations of sub-PeV and PeV emission from illuminated complexes such as W51, the Cygnus superbubble, and the orphan source LHAASO J2108+5157. We examine the implications of the recent IceCube detection of high-energy neutrinos from the Galactic plane at 4.5σ significance and discuss theoretical predictions for the neutrino flux from giant molecular cloud populations. Finally, we assess the prospects for next-generation multimessenger studies with CTAO and SWGO in the gamma-ray band and with IceCube-Gen2 and KM3NeT/ARCA in the neutrino channel, highlighting the synergies between these facilities that will be decisive for identifying the sources of Galactic cosmic rays up to and beyond the PeV regime.

Keywords: cosmic rays; molecular clouds; multimessenger astronomy; Galactic PeVatrons; high-energy neutrinos; very high energy gamma rays

1. Introduction

The origin of cosmic rays (CRs) is one of the longest-standing open questions in high-energy astrophysics. Since their discovery more than a century ago, the identification of the Galactic sources responsible for accelerating CR nuclei to energies up to the *knee* at a few PeV has remained elusive [1–3]. Because CR protons and heavier nuclei are deflected by interstellar magnetic fields during propagation, they carry no directional information about their origin by the time they reach Earth. Neutral messengers, gamma rays, and neutrinos produced by CR interactions near or within their sources, therefore, constitute the primary observational handle for tracing hadronic acceleration sites [1,4].

When relativistic protons interact with ambient matter through inelastic pp collisions, they produce charged and neutral pions. While π^0 decays produce gamma rays, the decay chain $\pi^{\pm} \to \mu^{\pm} + \nu_{\mu}(\bar{\nu}_{\mu}) \to e^{\pm} + \nu_e(\bar{\nu}_e) + \nu_{\mu} + \bar{\nu}_{\mu}$

generates neutrinos. This coupled gamma-ray and neutrino emission constitutes the hadronic multimessenger signature [5], and its unambiguous detection requires both gamma-ray telescopes and large-volume neutrino detectors working in concert.

Giant molecular clouds (GMCs) are massive concentrations of cold, dense interstellar gas, with typical masses of 10^4–$10^6\,M_\odot$ and number densities of $n \sim 10^2$–$10^3\,\mathrm{cm}^{-3}$, representing the dominant reservoir of molecular hydrogen in the Milky Way [6]. Because of their high target densities, GMCs provide extremely favorable conditions for hadronic interactions: cosmic rays injected into or propagating through these structures efficiently produce secondary gamma rays and neutrinos via pp processes. In this sense, GMCs can function as natural hadronic interaction targets [1], though the efficiency of energy conversion into secondary gamma rays and neutrinos depends critically on the ratio of the proton-proton cooling time to the CR confinement or escape time within the cloud, a ratio that varies by orders of magnitude across different cloud environments and CR energies (see Section 2.3). The resulting multimessenger emission encodes information on both the CR spectrum local to the cloud and the properties of nearby accelerators.

The interest in GMCs as multimessenger targets has grown substantially in the last decade, driven by major advances on three observational fronts. First, the Fermi Large Area Telescope (Fermi-LAT) has mapped GeV gamma-ray emission from numerous molecular cloud complexes, revealing hadronic spectral signatures such as the neutral pion bump and providing systematic constraints on the CR density across the Galaxy [7,8]. Second, ground-based gamma-ray observatories, most notably the High-Altitude Water Cherenkov Observatory (HAWC) and the Large High Altitude Air Shower Observatory (LHAASO), have extended these measurements to the very-high-energy (VHE; $E > 100\,\mathrm{GeV}$) and ultra-high-energy (UHE; $E > 100\,\mathrm{TeV}$) regimes, uncovering spatially extended emission from molecular cloud complexes coincident with candidate PeVatrons [9,10]. The detection of UHE gamma rays from W51, the Cygnus Cocoon, and dark sources such as LHAASO J2108+5157 has reinforced the picture of CR-illuminated molecular clouds as bright sources of hadronic emission at the highest energies [11,12]. Third, in 2023, the IceCube Neutrino Observatory reported the observation of high-energy neutrino emission from the Galactic plane at 4.5σ significance [13], directly confirming that hadronic CR interactions with interstellar gas, including GMCs, produce a detectable neutrino flux. Modeling studies have shown that a population of GMCs with a space-dependent CR distribution can account for a substantial fraction of this observed Galactic neutrino flux [14].

Beyond their role as passive targets for CR protons from external accelerators, molecular clouds are also deeply embedded in, or physically associated with, some of the most powerful CR factories in the Galaxy. Supernova remnants (SNRs), young massive stellar clusters (YMSCs), and pulsar wind nebulae (PWNe) are often found in proximity to GMCs, and the interplay between CR escape from these sources and subsequent diffusion into adjacent clouds is a key ingredient in understanding Galactic CR transport [15]. In the illuminated cloud scenario, CRs that have escaped from a nearby SNR or YMSC diffuse into a GMC and produce a gamma-ray and neutrino signal that reflects the accumulated history of CR injection rather than instantaneous acceleration [16]. Constraining the diffusion coefficient and spectral index of the escaping CRs through multimessenger observations of the cloud thus provides unique leverage on the broader problem of CR acceleration and propagation in the interstellar medium.

Looking forward, the next decade will bring transformative improvements in sensitivity across all multimessenger channels. The Cherenkov Telescope Array Observatory (CTAO) will achieve unprecedented angular resolution and sensitivity in the VHE band (0.1–$300\,\mathrm{TeV}$), enabling spatially resolved studies of CR-cloud interactions [17]. In the neutrino sector, IceCube-Gen2, KM3NeT, and Baikal-GVD will extend the reach of neutrino astronomy by roughly an order of magnitude [18,19]. The Southern Wide-field Gamma-ray Observatory (SWGO) will provide wide-field coverage of the Southern sky, including the Galactic center and inner Galaxy, where GMC populations are densest [20–22]. Combined, these facilities will transform GMCs from illustrative examples of hadronic emission into precision multimessenger laboratories.

This review is organized as follows. Section 2 describes the relevant physics of CR interactions in dense molecular gas, including proton-proton cross sections, pion production, gamma-ray and neutrino spectral modeling, CR transport, and diffusion inside and around clouds, as well as the role of low-energy cosmic rays in cloud ionization chemistry. Section 3 surveys gamma-ray observations of GMCs across three energy regimes: GeV observations by Fermi-LAT, VHE observations by H.E.S.S. and other IACTs, and UHE observations by LHAASO and HAWC. Section 4 discusses the theoretical predictions for neutrino emission from GMC populations, examines the implications of the IceCube detection of Galactic plane neutrinos, and reviews current constraints and future prospects from IceCube-Gen2 and KM3NeT/ARCA. Section 5 presents four illuminated-cloud case studies: the W51 complex, the Cygnus superbubble, the Central Molecular Zone, and LHAASO J2108+5157, as representative examples of the diversity of SNR-cloud and PeVatron-cloud interaction scenarios. Section 6 outlines the prospects for next-generation multimessenger studies with CTAO, SWGO, IceCube-Gen2, and KM3NeT/ARCA, including their

synergies with molecular line surveys. Section 7 summarizes the main conclusions and discusses the outstanding open questions in the field.

2. Physical Mechanisms of Hadronic Interactions in Molecular Clouds

Molecular clouds are among the densest structures in the interstellar medium (ISM), with hydrogen number densities ranging from $n \sim 10^2\,\mathrm{cm}^{-3}$ in the diffuse outer envelopes to $n \sim 10^5\,\mathrm{cm}^{-3}$ in the dense cores of GMCs [6,23]. This high target density makes them exceptionally efficient interaction sites for CR protons and heavier nuclei. In this section, we describe the physics underlying the hadronic multimessenger emission from these environments, starting from the microphysics of proton-proton collisions, proceeding through the derivation of the resulting gamma-ray and neutrino spectra, and concluding with the macroscopic problem of CR transport and diffusion inside and around the clouds.

2.1. Proton-Proton Interactions and Pion Production

The dominant hadronic process in the dense, cold gas of a molecular cloud is the inelastic collision between a relativistic CR proton and a proton (or nucleus) in the ambient medium. For a CR proton with kinetic energy T_p above the kinematic threshold for pion production, $T_p^{\mathrm{th}} = 2m_\pi + m_\pi^2/2m_p \approx 0.28\,\mathrm{GeV}$, the reaction

$$p + p \longrightarrow p + p + a\,\pi^0 + b\,(\pi^+ + \pi^-), \tag{1}$$

produces neutral and charged pions with multiplicities a and b that grow slowly with energy [24]. The inelastic cross section for this process rises logarithmically with proton energy, from $\sigma_{pp}^{\mathrm{inel}} \approx 30\,\mathrm{mb}$ near threshold to approximately $40\,\mathrm{mb}$ at GeV energies and $\sim 60\,\mathrm{mb}$ at PeV energies [3,25]. For astrophysical modeling purposes, accurate parametrizations of $\sigma_{pp}^{\mathrm{inel}}$ covering the full range from the kinematic threshold to PeV energies are available in the literature [24–26], with the widely adopted formulation of Kafexhiu et al. [25] providing an accuracy better than 20% across this entire range.

The subsequent decay of the produced pions determines the multimessenger output, as illustrated schematically in Figure 1. Neutral pions decay almost immediately ($c\tau \approx 25\,\mathrm{nm}$) into two photons,

$$\pi^0 \longrightarrow \gamma + \gamma, \tag{2}$$

generating a gamma-ray spectrum with a characteristic spectral feature, the so-called pion-decay bump, centered at $E_\gamma = m_{\pi^0}/2 \approx 67.5\,\mathrm{MeV}$ in the rest frame of the pion and appearing as a low-energy spectral break in the observed gamma-ray SED [27]. This morphological feature is a smoking-gun diagnostic of hadronic CR interactions in the source region and has been directly observed by the Fermi-LAT in several SNR-cloud interaction systems [27]. As shown in Figure 1, charged pions decay through the chain

$$\pi^\pm \longrightarrow \mu^\pm + \nu_\mu\,(\bar{\nu}_\mu) \longrightarrow e^\pm + \nu_e\,(\bar{\nu}_e) + \nu_\mu + \bar{\nu}_\mu, \tag{3}$$

producing three neutrinos (or antineutrinos) per charged pion, along with an electron or positron. The hadronic cascade also feeds a third branch visible in the figure: spallation reactions produce nuclear fragments, neutrons, and heavier secondary hadrons that contribute to the ionizing particle flux in the cloud interior, connecting the high-energy multimessenger emission to the low-energy CR ionization chemistry discussed in Section 2.4. Because charged and neutral pions are produced roughly in a ratio $\pi^\pm : \pi^0 \approx 2 : 1$ at high energies (though this ratio depends on energy, particularly near threshold), the gamma-ray and neutrino luminosities are intrinsically linked. Specifically, for a fully transparent source, the total all-flavor neutrino energy flux is expected to be approximately twice the gamma-ray energy flux produced by the same hadronic interactions [1,24]. This fundamental connection constitutes the theoretical basis for multimessenger predictions and consistency checks.

2.2. Gamma-Ray and Neutrino Spectral Modeling

The observed gamma-ray spectrum from a molecular cloud illuminated by cosmic rays is obtained by convolving the differential CR proton spectrum $N_p(E_p)$ with the differential cross section for gamma-ray production. In the standard formulation, this assumes: (i) a steady-state CR distribution that has had time to fill the cloud uniformly; (ii) a spatially homogeneous target gas density n_{gas}; (iii) an isotropic and spatially uniform CR flux within the cloud volume; and (iv) negligible energy losses of the CR protons while traversing the cloud (the so-called thin-target or transparent limit). These assumptions are good approximations when the proton-proton cooling time t_{pp} greatly exceeds the CR residence time in the cloud, but they break down progressively as the cloud density

increases or the CR confinement timescale grows, as discussed below. Under these conditions, and taking the CR proton spectrum as a power law $N_p(E_p) \propto E_p^{-\Gamma}$ with a spectral index $\Gamma \approx 2.0$–2.7 depending on the proximity to the accelerator [28,29], the emissivity is

$$\frac{dN_\gamma}{dE_\gamma} = c\, n_{\rm gas} \int_{E_\gamma}^{\infty} N_p(E_p)\, \frac{d\sigma_\gamma(E_p, E_\gamma)}{dE_\gamma}\, dE_p\,, \tag{4}$$

where $n_{\rm gas}$ is the number density of the target gas, c is the speed of light, and $d\sigma_\gamma/dE_\gamma$ is the differential cross section for gamma ray production in pp collisions [24,25]. The parametrization of Kelner, Aharonian, & Bugayov [24]. This provides accurate analytical expressions for the spectra of gamma rays, electrons, and neutrinos at proton energies above $\sim 100\,\mathrm{GeV}$, while the more recent work of Kafexhiu et al. [25] extends the calculation from the kinematic threshold to PeV energies, making it particularly important for modeling the sub-GeV spectral structure around the pion-decay bump.

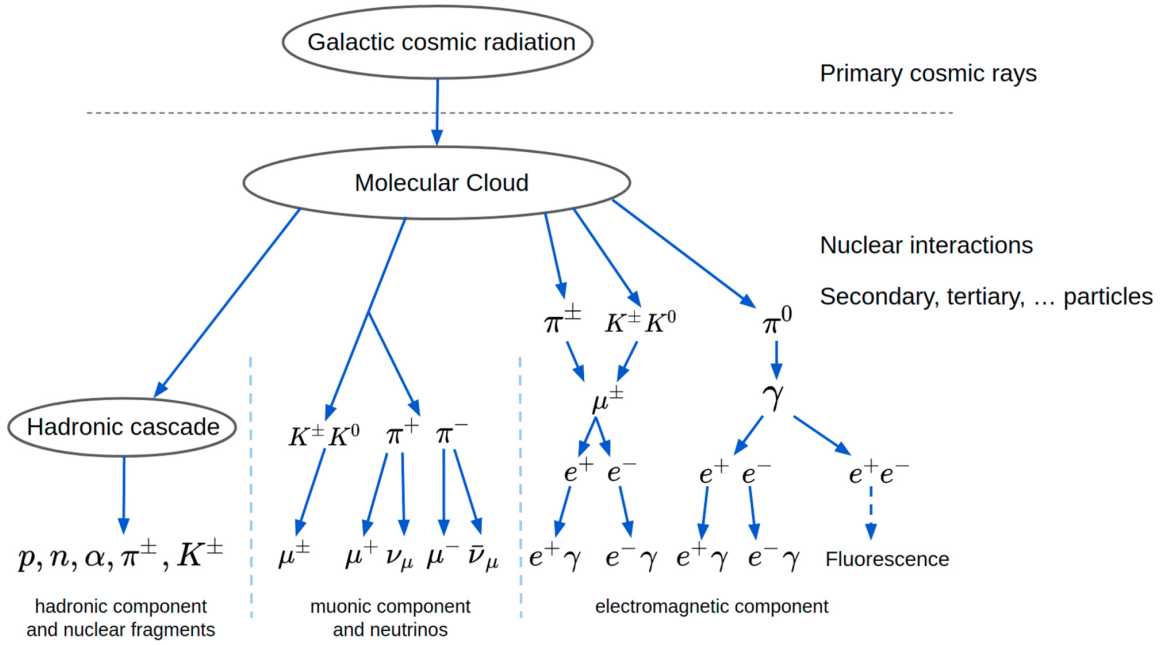

Figure 1. Schematic diagram of the CR-induced particle cascade initiated when primary Galactic cosmic rays interact with the gas of a molecular cloud (H_2 gas phase and solid-phase C grains). The three branches of the cascade correspond to the hadronic component (nucleons, α particles, and nuclear fragments produced in spallation reactions), the muonic component and associated neutrinos (arising from the decay chain $\pi^\pm, K^\pm \to \mu^\pm \to e^\pm$), and the electromagnetic component (gamma rays, electrons, and positrons from π^0 decay and subsequent pair production and bremsstrahlung). The diagram illustrates the physical origin of the multimessenger connection reviewed in this work: a single hadronic interaction simultaneously feeds the gamma-ray channel through $\pi^0 \to \gamma\gamma$, the neutrino channel through $\pi^\pm \to \mu^\pm\nu \to e^\pm\nu\nu$, and the ionizing particle channel through the hadronic and electromagnetic sub-cascades. Reprinted from Pazianotto et al. [30].

A physically important quantity for characterizing the efficiency of hadronic interactions in a molecular cloud is the cooling time for proton-proton inelastic collisions [28,31],

$$t_{pp} \approx \frac{1}{\kappa_{pp}\, \sigma_{pp}^{\rm inel}\, n_{\rm gas}\, c} \approx 5.3 \times 10^7 \left(\frac{n_{\rm gas}}{1\,\mathrm{cm^{-3}}}\right)^{-1} \mathrm{yr}\,, \tag{5}$$

where $\kappa_{pp} \approx 0.5$ is the inelasticity coefficient, i.e., the average fraction of the proton kinetic energy transferred to secondaries per interaction [1,28]. For the diffuse ISM with $n \sim 1\,\mathrm{cm^{-3}}$, the cooling time is $t_{pp} \sim 5 \times 10^7$ yr, comparable to the CR confinement timescale in the Galaxy ($\sim 10^7$–10^8 yr) [29], meaning that only a small fraction of CR energy is lost to pp interactions in the diffuse ISM. For cloud envelopes with $n \sim 10^2\,\mathrm{cm^{-3}}$, t_{pp} drops to $\sim 5 \times 10^5$ yr, and for dense cores ($n \sim 10^3\,\mathrm{cm^{-3}}$) to $\sim 5 \times 10^4$ yr, both of which are much shorter than the Galactic confinement time. Whether a given cloud behaves as a thin target (transparent; $t_{pp} \gg t_{\rm esc}$), a partial calorimeter ($t_{pp} \sim t_{\rm esc}$), or approaches full calorimetry ($t_{pp} \ll t_{\rm esc}$) depends not only on density but critically on the CR escape or confinement time within the cloud itself, which is controlled by transport, diffusion coefficients, magnetic

topology, ion-neutral damping of Alfvén waves, and cloud substructure [32]. In the thin-target regime, the hadronic emission is proportional to $W_p \cdot n_{\rm gas}$, where W_p is the total energy in CR protons within the cloud, regardless of the column density. In the calorimetric limit, the emission saturates at a fraction of the total CR energy injection rate, set by the ratio $t_{\rm esc}/t_{pp}$. Intermediate, partially calorimetric regimes require a full transport treatment to relate the observed fluxes to the underlying CR source [28,33].

An important subtlety in modeling the gamma-ray emissivity concerns the contribution of nuclei heavier than hydrogen, both in the CR flux and in the ambient gas. Because both the CR beam and the ISM gas contain helium and heavier elements, the effective gamma-ray emissivity must be multiplied by a nuclear enhancement factor $\kappa_{\rm nuc} \approx 1.5$–$1.8$, which accounts for the higher pion multiplicity in nucleus-nucleus interactions compared to pure pp collisions [25,34]. This correction is particularly relevant for precision modeling in dense environments where accurate absolute flux predictions are required.

The expected neutrino spectrum follows directly from the same hadronic interaction chain. For each flavor, the differential neutrino emissivity is computed analogously to Equation (4), replacing $d\sigma_\gamma/dE_\gamma$ with the corresponding differential neutrino production cross section, which accounts for the kinematics of both the $\pi^\pm$ and $K^\pm$ decay chains [24]. At energies above $\sim 1\,\mathrm{TeV}$, kaon production becomes a significant additional neutrino source, as kaons are produced in abundance at high center-of-mass energies, and their leptonic decay channels yield high-energy neutrinos with harder spectra than pion-decay neutrinos [1,24]. For this reason, models that aim to predict the neutrino emission at TeV–PeV energies from clouds near PeVatrons must include kaon contributions [1,24]. After production, neutrinos propagate freely to the observer and undergo flavor oscillations, so that by the time they arrive at Earth, an initial flavor ratio of $\nu_e : \nu_\mu : \nu_\tau = 1 : 2 : 0$ at the source evolves to an approximately equal partition of $1 : 1 : 1$ [4].

2.3. Cosmic-Ray Transport in and Around Molecular Clouds

The multimessenger emission from a molecular cloud is sensitive not only to the hadronic cross sections described above but also, and often more critically, to how cosmic rays propagate from their acceleration sites into and through the cloud. The transport of CRs in the ISM is governed by a combination of spatial diffusion in the turbulent Galactic magnetic field, convective transport by plasma winds, adiabatic losses or gains due to gas flows, and energy losses through hadronic and ionization processes [29,33]. For CRs in the energy range of interest for gamma-ray and neutrino production (GeV to PeV), the dominant transport mechanism is diffusion, and the steady-state CR distribution around a localized source satisfies the diffusion equation,

$$\frac{\partial N_p}{\partial t} = \nabla \cdot [D(E)\,\nabla N_p] - \frac{N_p}{t_{pp}} + Q(E, \mathbf{r}, t), \tag{6}$$

where $D(E)$ is the energy-dependent diffusion coefficient and Q is the source term [28,29,35]. In the standard picture of Galactic CR propagation, the diffusion coefficient follows a power-law dependence on particle rigidity, $D(E) = D_0(E/E_0)^\delta$, with $D_0 \approx 3 \times 10^{28}\,\mathrm{cm^2\,s^{-1}}$ at $E_0 = 1\,\mathrm{GeV}$ and $\delta \approx 0.3$–0.6 depending on the assumed turbulence spectrum (Kolmogorov or Kraichnan) [28,29].

A crucial and physically rich complication arises from the fact that the diffusion coefficient inside a molecular cloud is likely substantially suppressed compared to the average Galactic value. Several mechanisms contribute to this suppression: the higher magnetic field strength in the cloud (which reduces the particle Larmor radius), the greater level of magnetohydrodynamic (MHD) turbulence generated by star formation and stellar winds within the cloud, and, most importantly, the self-confinement of CRs through the resonant excitation of Alfvén waves [36,37]. When CRs stream down a density gradient, they amplify the Alfvén waves through the streaming instability; the enhanced wave field then isotropizes the CR distribution and suppresses their net streaming speed. In practice, diffusion coefficients derived from gamma-ray observations of SNR-cloud associations are often found to be two orders of magnitude below the standard Galactic value, $D_{\rm cloud} \sim 10^{26}\,\mathrm{cm^2\,s^{-1}}$ at TeV energies, indicating strong local confinement of CRs in these environments [28,38].

This suppression has profound consequences for the observable gamma-ray and neutrino emission. As shown by Gabici, Aharonian, & Blasi [28], if the diffusion coefficient inside the cloud is significantly smaller than outside, low-energy CRs have difficulty penetrating to the cloud core, while higher-energy CRs, which diffuse faster, can traverse the cloud more readily. The net result is that the CR spectrum inside the cloud is harder than outside, leading to a gamma-ray spectrum that appears harder than the injection spectrum of the parent accelerator. This energy-dependent exclusion effect produces a characteristic spectral shape that can potentially be used to diagnose the diffusion regime inside the cloud [28,33].

In the case of the passive or illuminated-cloud scenario, where the cloud is not adjacent to a current accelerator but is instead bathed in the sea of Galactic CR background, the situation is simpler. The CR spectrum inside the

cloud can be taken to be equal to the local interstellar spectrum, and the gamma-ray emissivity is simply proportional to the product of the cloud column density and the local CR energy density [6,33]. In this passive case, molecular clouds act as cosmic-ray barometers, allowing the spatial distribution of CRs across the Galaxy to be mapped through gamma-ray observations. Indeed, Fermi-LAT has used this approach to constrain CR gradients in the Galactic disk, finding evidence for harder CR spectra in the inner Galaxy consistent with a higher density of CR sources near the Galactic center [7].

In the active scenario, where a nearby accelerator such as an SNR, a YMSC, or a PWN injects an excess of CRs into the surrounding medium, the gamma-ray and neutrino output of the adjacent cloud can significantly exceed the passive level. The time evolution of this emission reflects the history of CR injection and the properties of diffusion in the ISM between the source and the cloud. In the simplest one-zone model, the CR density at a cloud located at a distance d from the accelerator at a time t after the injection event is [16,28]

$$N_p(E, d, t) \propto \frac{Q_0(E)}{[4\pi D(E)t]^{3/2}} \exp\left(-\frac{d^2}{4D(E)t}\right), \tag{7}$$

where $Q_0(E)$ is the total energy injected per unit energy by the source. This Gaussian diffusion profile implies that the CR overdensity around the source forms an expanding halo with a characteristic diffusion radius $R_d(t) = \sqrt{4D(E)t}$. When $R_d > d$, the cloud is effectively engulfed by the CR halo, and its multimessenger emission is strongly enhanced above the passive background level. Gamma-ray and neutrino observations of clouds at known distances from identified accelerators can therefore be used to constrain the product $\eta_{\rm CR}/D^{3/2}$, where $\eta_{\rm CR}$ is the CR acceleration efficiency of the source [28,33,39].

2.4. Low-Energy Cosmic Rays and Cloud Chemistry

While the high-energy end of the CR spectrum ($E \gtrsim 1\,\mathrm{GeV}$) is primarily responsible for the pion-decay gamma-ray and neutrino emission discussed above, low-energy cosmic rays (LECRs) with energies below $\sim 1\,\mathrm{GeV}$ have a distinct and equally important impact on the physical state of molecular clouds [40,41]. These sub-GeV particles dominate the ionization of molecular gas in the cloud interiors, where UV radiation cannot penetrate. The CR ionization rate $\zeta_{\rm CR}$, typically on the order of 10^{-17}–$10^{-15}\,\mathrm{s}^{-1}$ per H_2 molecule [41], controls the degree of ionization of the gas, which in turn regulates the coupling between the gas and the magnetic field, the rate of ambipolar diffusion, the efficiency of protostellar accretion, and the network of ion-molecule chemical reactions that determine the molecular composition of the cloud [40].

From a multimessenger perspective, LECRs interacting with molecular gas through inelastic nuclear excitation reactions produce a distinct emission signature in the MeV band: narrow nuclear de-excitation lines and a broad continuum of bremsstrahlung radiation from secondary electrons [42]. These features, predicted to arise particularly in clouds near powerful CR sources or in the Galactic center region, are expected to be detectable by the next generation of MeV Gamma-ray telescopes, such as the All-sky Medium Energy Gamma-ray Observatory eXplorer (AMEGO-X) and the Compton Spectrometer and Imager (COSI) [42]. Including the LECR contribution thus extends the multimessenger picture of molecular clouds from the MeV to the PeV energy decade, covering more than seven orders of magnitude in photon energy and offering complementary diagnostics on the CR spectrum at all energies.

2.5. Summary of the Physical Picture

Taking stock of the various processes described in this section, the multimessenger emission from a molecular cloud can be understood as a hierarchical interplay between microphysics and macrophysics. At the microscopic level, the *pp* cross section and pion kinematics determine the spectral shapes of the gamma-ray and neutrino outputs and link them to the parent CR spectrum through well-calibrated parameterizations [24,25]. At the macroscopic level, the spatial distribution of CRs within and around the cloud, controlled by diffusion in the turbulent magnetic field and by the history of the nearby accelerators, modulates the overall normalization and spectral shape of the emission [28,33]. The column density and total mass of the cloud set the scaling of the emission, while its distance and angular size determine observability with current and future instruments. The interplay of all these factors means that molecular clouds are not merely passive targets; they are multimessenger laboratories encoding information on CR acceleration, CR transport, and the ISM physics of the Galaxy simultaneously.

3. Gamma-Ray Observations of Molecular Clouds

The gamma-ray sky has proven to be an extraordinarily rich window onto the physics of cosmic-ray interactions with molecular gas. Over the past two decades, observations spanning more than six decades in photon energy, from

the sub-GeV domain accessible to space-borne pair-conversion telescopes up to the sub-PeV frontier reached by ground-based particle-detector arrays, have transformed molecular clouds from passive tracers of the interstellar medium into central actors in the multi-messenger story of cosmic-ray origin and transport. This section reviews the observational landscape, organized by energy regime and by the physical role attributed to the clouds.

3.1. The GeV Window: Fermi-LAT and the CR Barometer Programme

The Fermi-LAT, operating since 2008, has produced the most systematic census of GeV gamma-ray emission from molecular gas in the Galaxy. Two distinct observational programs have emerged from Fermi-LAT data, each probing a different astrophysical regime.

The first concerns clouds in direct physical interaction with SNR shocks. The landmark result in this category came from the detection of the characteristic pion-decay spectral feature, a low-energy break near $\sim$200 MeV caused by the kinematic threshold of neutral pion production, in the spectra of the SNRs IC 443 and W 44 [27]. Both remnants are embedded in dense molecular environments with number densities $n \gtrsim 10^2$–$10^3\,\mathrm{cm}^{-3}$ [27, 28], providing abundant target material for hadronic collisions. As shown in Figure 2, the observed spectral hardening below $\sim$200 MeV, the so-called pion-decay bump, is reproduced by hadronic (π^0-decay) models but cannot be accounted for by bremsstrahlung or inverse Compton scenarios without invoking physically extreme electron spectra [27]. This constitutes the most direct observational evidence to date that supernova remnants accelerate cosmic-ray protons. The gamma-ray luminosities of these SNR-cloud systems reach $L_\gamma \sim 10^{35}$–$10^{36}\,\mathrm{erg\,s}^{-1}$ [27,43,44], consistent with hadronic models in which a fraction $\eta \approx 10\%$ of the canonical supernova kinetic energy $E_{\mathrm{SN}} \approx 10^{51}$ erg is transferred to relativistic protons interacting with the shocked molecular gas [28].

The second Fermi-LAT program exploits passive molecular clouds, which are not directly illuminated by a nearby accelerator but are rather immersed in the large-scale galactic cosmic-ray sea and serve as CR barometers [45–47]. Since the gamma-ray emissivity of a passive cloud depends only on the local CR proton density (see Section 2.2), clouds at different Galactocentric radii can be used to map the radial gradient of the CR density across the Galaxy. Fermi-LAT analysis of the galactic interstellar emission model confirmed that the CR proton density decreases with Galactocentric distance beyond $\sim$5 kpc from the Galactic Center [7], broadly consistent with the expected distribution of SNR sources in the Galactic disk. A more targeted study subsequently analyzed nine individual clouds in the 1.5–4.5 kpc Galactocentric range using 11 years of LAT data, finding that the CR density at each cloud location is compatible with the locally measured value and concluding that the apparent gamma-ray gradient seen in diffuse emission maps is driven by the presence of active CR accelerators in the inner Galaxy rather than by a global change in CR propagation [8]. This distinction is physically important, it implies that the Galactic CR "sea" is approximately uniform on large scales, while local enhancements trace individual injection events.

The Gould Belt molecular clouds, including Ophiuchus, Perseus, Orion, and Taurus, have been detected by Fermi-LAT at GeV energies consistent with passive illumination by the local CR sea [46–49]. A comparative study of eight clouds in the Gould Belt demonstrated that their gamma-ray luminosities scale strongly with gas mass but show no significant correlation with the local star-formation rate, in contrast to star-forming galaxies, whose gamma-ray emission scales with star-formation activity [7]. This mass-luminosity proportionality is precisely the signature of hadronic emission from diffuse CR penetration, confirming that the Gould Belt clouds serve as faithful probes of the ambient CR spectrum.

3.2. The TeV Regime: HESS, MAGIC, VERITAS, and the Illuminated-Cloud Scenario

At very high energies (VHE; $E > 100$ GeV), imaging atmospheric Cherenkov telescopes (IACTs) have resolved spatially extended gamma-ray emission from several SNR–cloud complexes, allowing the geometry of CR diffusion from the accelerator into the surrounding gas to be constrained observationally [38, 50, 51]. The paradigmatic case is W 28, where H.E.S.S. detected VHE emission from two discrete molecular cloud complexes located to the northeast and south of the SNR shell [28]. The offset between the SNR boundary and the centroid of gamma-ray emission is a direct consequence of CR diffusion: particles that have already escaped the shock illuminate external gas after traveling distances $r_d \sim \sqrt{4D(E)t} \approx 10$–$100$ pc, where $D(E)$ is the energy-dependent diffusion coefficient and t is the age of the remnant [15, 38]. Modeling of the W 28 system yields diffusion coefficients at TeV energies on the order of $D \sim 10^{26}$–$10^{27}\,\mathrm{cm}^2\,\mathrm{s}^{-1}$, which is more than an order of magnitude below the Galactic average [38], providing strong evidence for CR self-confinement through streaming instability near active accelerators.

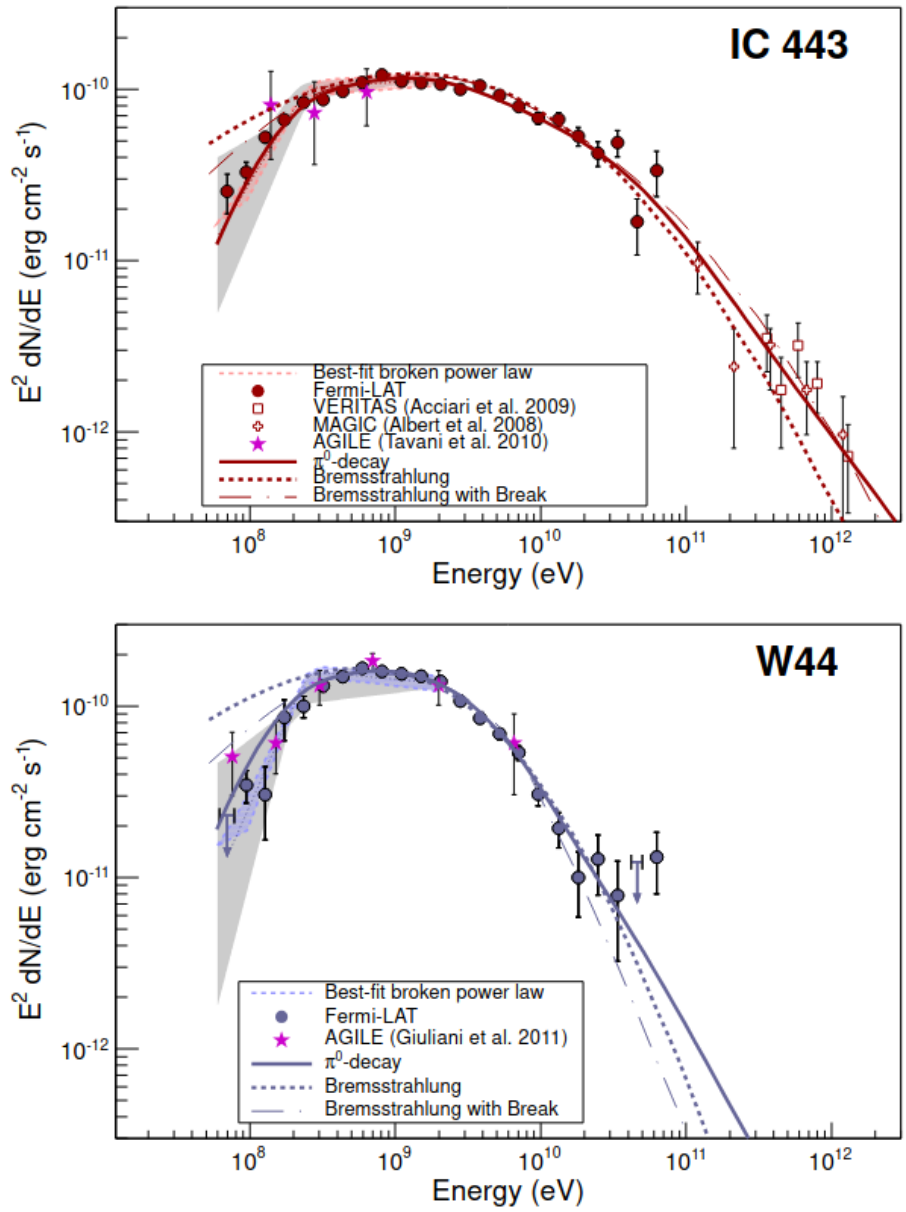

Figure 2. Gamma-ray spectral energy distributions of SNR IC 443 (**top**) and W 44 (**bottom**) measured by Fermi-LAT [27]. Data points are shown with statistical uncertainties. The solid lines show the best-fit hadronic (π^0-decay) models, where the parent proton spectrum is described by a smoothly broken power law; the dashed and dash-dotted lines show bremsstrahlung models with and without a low-energy break in the electron spectrum, respectively. The sharp spectral hardening below ∼200 MeV, the so-called pion-decay bump at ∼67.5 MeV, cannot be reproduced by any physically motivated leptonic scenario, providing direct evidence that cosmic-ray protons are accelerated in supernova remnants interacting with molecular gas. Reprinted with permission from Ref [27], Copyright 2026, Science.

The W 51 complex, one of the most massive star-forming regions in the inner Galaxy, has been detected from GeV to TeV energies. At GeV, Fermi-LAT revealed emission consistent with hadronic interactions of CRs accelerated by SNR W 51C with the adjacent molecular cloud complex W 51B. The power-law spectrum extending to tens of GeV without a cutoff suggests that particles are being accelerated well beyond the TeV range [52,53].

3.3. Ultra-High-Energy Gamma Rays: LHAASO and the PeVatron Connection

The commissioning of LHAASO on Haizi Mountain (Sichuan, China) at 4410 m altitude has opened the sub-PeV energy window to a systematic survey, revealing a population of ultra-high-energy (UHE; $E > 100$ TeV) gamma-ray sources in the Galactic plane [9]. A substantial fraction of these sources lacks counterparts in classical high-energy catalogs; yet, they are spatially coincident with massive molecular cloud complexes, pointing to the illuminated-cloud scenario as their natural physical explanation.

The first LHAASO catalog [10] contains 90 sources detected above 25 TeV (Figure 3), with 43 sources reaching

energies above 100 TeV. Several of these are in crowded star-forming environments, where the association with individual molecular clouds or cloud complexes is geometrically compelling. The prototypical case is LHAASO J2108+5157, detected without a convincing counterpart in the radio, X-ray, or GeV bands, yet spatially coincident with CO-emitting molecular gas in the Cygnus OB7 association [11]. Modeling this source as a cloud illuminated by CRs escaping from a nearby SNR reproduces the observed UHE spectrum and constrains the required diffusion suppression to $D_{\rm cloud} \sim 10^{25}$–$10^{26}$ cm^2 s^{-1}, consistent with the picture of CR self-trapping discussed in Section 2.3.

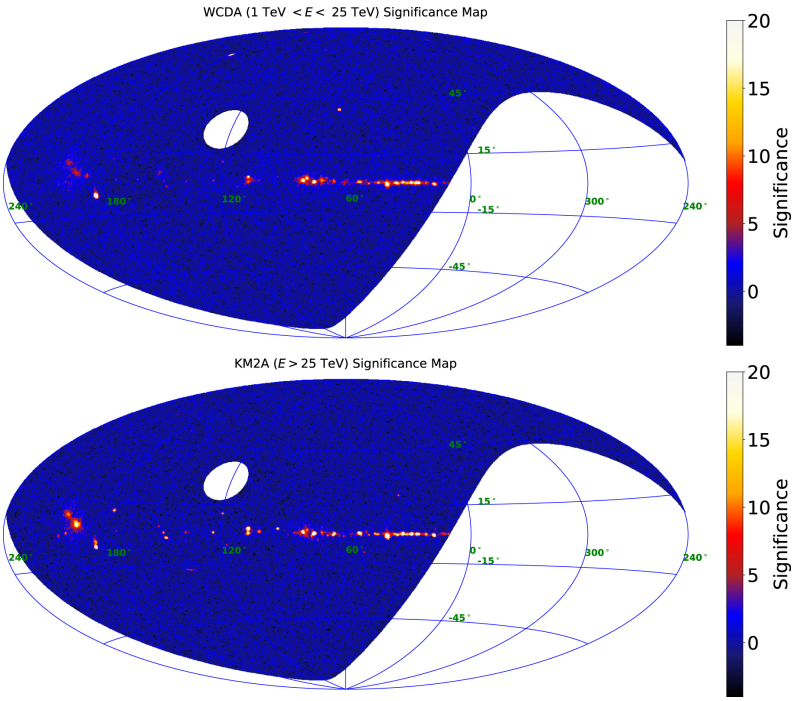

Figure 3. All-sky significance maps of the region surveyed by LHAASO in Galactic coordinates. **Top panel**: WCDA map in the energy band $1\,\mathrm{TeV} < E < 25\,\mathrm{TeV}$, using a point-source test with spectral index $\Gamma = 2.6$. **Bottom panel**: KM2A map at $E > 25\,\mathrm{TeV}$, using $\Gamma = 3.0$. The survey covers declinations from -20° to 80° and contains 90 sources with significance $> 5\sigma$ and angular extension $< 2^\circ$, of which 43 are detected as ultra-high-energy (UHE) sources with $E > 100\,\mathrm{TeV}$ at $> 4\sigma$ significance. Concentrations of sources along the inner Galactic plane are consistent with hadronic interactions of cosmic rays with dense molecular gas acting as target material. Reprinted from Cao et al. [10].

One of the most spectacular results from LHAASO concerns the Cygnus X star-forming region, where a giant UHE gamma-ray bubble spanning at least $100\,\mathrm{deg}^2$ was detected, with multiple photons exceeding 1 PeV and the highest-energy photon reaching 2.5 PeV [10]. The spatial distribution of UHE emission within this bubble is not uniform: "hot spots" correlated with the positions of massive molecular clouds are observed against the smoother bubble background, providing direct morphological evidence that molecular gas acts as the hadronic target converting CR energy into gamma rays. The central candidate accelerator is the OB association Cygnus OB2, making this the first identified super PeVatron, an accelerator capable of boosting particles beyond 10 PeV and continuously injecting them into the surrounding medium. The gamma-ray bubble has a counterpart at GeV energies in the Fermi-LAT-discovered Cygnus Cocoon, establishing spectral and spatial continuity from $\sim$1 GeV to several PeV and constraining the CR spectral index in the source region to $\Gamma \approx 2.3$–2.4 [10].

The W 51 complex provides a complementary case at somewhat lower energies. LHAASO detected gamma-ray emission from W 51 extending from 2 TeV up to ~ 200 TeV, revealing a spectral break at tens of TeV that, when modeled as a simple pp-collision spectrum, implies an exponential cutoff in the parent CR proton spectrum at $E^{\rm p}_{\rm cut} \sim 200$ TeV [12]. This spectral bending provides the first observational evidence that an individual SNR, W 51C, is accelerating protons approaching the PeV regime, but not yet reaching it, offering a lower energy anchor for the PeVatron population that LHAASO is beginning to map across the Galaxy.

3.4. Diffuse Emission and the Large-Scale CR Gradient

Beyond individual cloud associations, molecular gas contributes substantially to the large-scale diffuse gamma-ray emission of the Galactic plane. Fermi-LAT maps of this diffuse emission are constructed by decomposing the

sky brightness into contributions from HI and CO-traced gas in Galactocentric annuli, inverse Compton emission from relativistic electrons, and point sources [7]. The emissivity per hydrogen atom derived from this decomposition, which is proportional to the local CR proton density, decreases by a factor of ∼3–5 from the 4 kpc molecular ring to the outer Galaxy beyond 10 kpc, confirming the Galactic gradient of CR density that propagation models based on a distributed SNR source population predict [29]. However, as individual cloud studies have demonstrated, this apparent gradient is not uniform: molecular clouds in the inner Galaxy show CR densities compatible with the locally measured solar neighborhood value, suggesting that enhanced emissivity near the 4 kpc ring traces an over-density of active CR accelerators rather than a systematic enhancement of the CR sea itself [8].

At TeV energies and above, the galactic diffuse emission remains less well characterized, though LHAASO measurements of the Galactic plane indicate that the sub-PeV diffuse flux is dominated by hadronic interactions, with contributions from both truly diffuse emission (CR sea interacting with the molecular ISM) and the unresolved tails of discrete source populations [54,55]. Disentangling these components and quantifying the fraction of the UHE diffuse emission that arises from molecular cloud target gas is one of the central observational challenges for the coming decade to be addressed by CTAO and SWGO in the southern sky [17,20,22].

3.5. Summary of Observational Constraints

Taken together, the observational record from Fermi-LAT through LHAASO establishes a coherent picture in which molecular clouds participate in three distinct gamma-ray production regimes. In the first, clouds are crushed or overrun by SNR shocks, producing bright GeV–TeV emission whose spectrum carries the pion-decay signature that uniquely identifies hadronic interactions; IC 443, W 44, W 28, and W 51 are the best-studied examples [27,28]. In the second, clouds are passively illuminated by the large-scale galactic CR sea, and their gamma-ray emissivity directly traces the local CR proton density, making them precision barometers of CR transport on Galactic scales [7,8]. In the third, the regime newly opened by LHAASO, clouds serve as hadronic calorimeters for ultra-energetic particles escaping from nearby PeVatrons, with the spatial correlation between UHE hot spots and molecular gas offering perhaps the cleanest available evidence that particle acceleration to PeV energies is occurring in the Galaxy [9–12]. Each of these regimes is characterized by a different relationship between the cloud and the CR source, a distinction that will be explored through specific astrophysical scenarios in Section 5.

4. Neutrino Emission from Molecular Clouds

The hadronic interactions responsible for the gamma-ray emission reviewed in Section 3 inevitably produce high-energy neutrinos through the charged-pion channel (Section 2.1). For every $\pi^0 \to \gamma\gamma$ decay, there are, on average, two charged pions, each yielding three neutrinos via $\pi^\pm \to \mu^\pm + \nu_\mu(\bar{\nu}_\mu) \to e^\pm + \nu_e(\bar{\nu}_e) + \nu_\mu + \bar{\nu}_\mu$. After vacuum oscillations over astrophysical baselines, the initial flavor ratio $(1:2:0)$ at the source equilibrates to $(1:1:1)$ at Earth [1], so that the $\nu_\mu + \bar{\nu}_\mu$ flux detectable through muon-track events is one-third of the total neutrino output. The expected $\nu_\mu + \bar{\nu}_\mu$ energy flux is linked to the gamma-ray flux by

$$E_\nu^2 \Phi_{\nu_\mu+\bar{\nu}_\mu}(E_\nu) \;\approx\; \frac{1}{2}\, E_\gamma^2 \Phi_\gamma(E_\gamma)\Big|_{E_\gamma = 2E_\nu}, \tag{8}$$

which follows from the near-equal energy sharing among the four leptons produced per $\pi^\pm$ decay [24]. This tight coupling means that every confirmed hadronic gamma-ray emitter is, by construction, also a neutrino source, even if individual clouds often lie below current detector thresholds. The kaon contribution to the charged secondary spectrum becomes relevant above ∼1 TeV and slightly modifies the spectral index of the predicted neutrino flux relative to a pure pion-only calculation; it is included in modern parameterizations [24,25].

4.1. The Galactic Plane Detection by IceCube

For decades, diffuse neutrino emission from the Galactic plane was predicted by propagation models but remained undetected. This situation changed in June 2023 when the IceCube Collaboration reported the observation of high-energy neutrino emission from the Milky Way at 4.5σ significance, using ten years of data processed with machine-learning event reconstruction [13]. Three spatial templates were compared against a background-only hypothesis: the π^0-decay template derived from Fermi-LAT gamma-ray maps [56] and two KRA$_\gamma$ models built on DRAGON cosmic-ray propagation [57,58]. The highest significance was obtained with the π^0 template, lending direct support to a hadronic interpretation in which molecular gas serves as the dominant interaction target [13].

As shown in Figure 4, the neutrino flux reconstructed by IceCube is consistent with the pionic gamma-ray emission measured by Fermi-LAT at GeV energies [56] and by Tibet ASγ near ∼0.5 PeV [59], spanning nearly five decades in energy [13]. This multimessenger consistency supports the conclusion that hadronic interactions

dominate the diffuse gamma-ray emission above ∼1 TeV [13]. The signal could arise from a genuinely diffuse component, from a population of unresolved point sources along the plane, or from a mixture of both; distinguishing these scenarios is one of the principal goals of next-generation detectors [13,60].

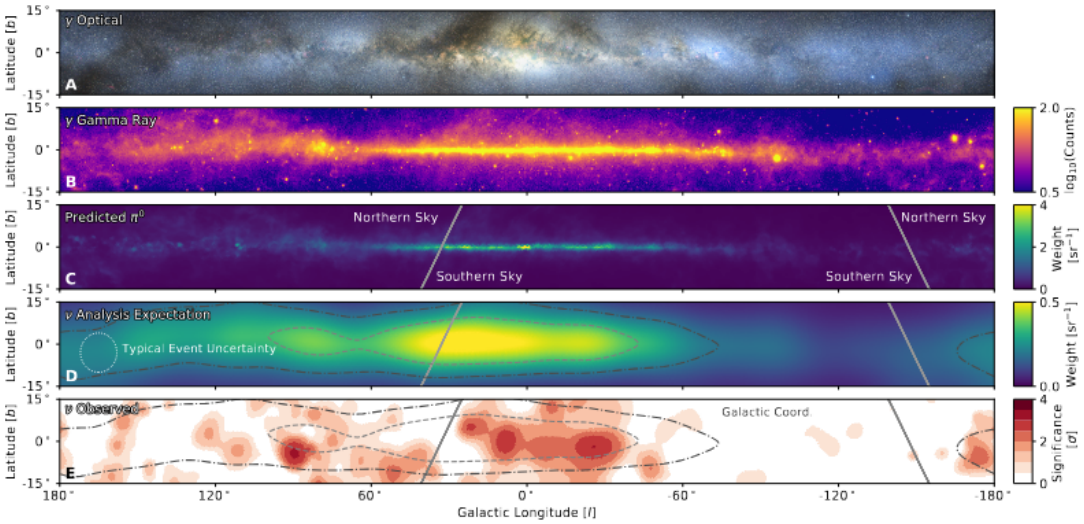

Figure 4. The Galactic plane in photons and neutrinos, in Galactic coordinates centred on the Galactic Centre and extending $\pm 15^\circ$ in latitude. (**A**) Optical image of the Milky Way (credit: A. Mellinger). (**B**) Integrated gamma-ray flux from the 12-year Fermi-LAT survey above 1 GeV. (**C**) Predicted neutrino emission template derived from the π^0-decay model fit to the Fermi-LAT diffuse gamma-ray emission; grey lines mark the IceCube Northern/Southern sky boundary. (**D**) Analysis expectation after folding panel (**C**) with the IceCube cascade event sensitivity and the 7° typical angular uncertainty (dotted circle); contours enclose the regions contributing 20% and 50% of the predicted signal. (**E**) Pre-trial significance of the observed IceCube neutrino signal from the all-sky point-source scan. The spatial correlation between the observed excess in panel (**E**) and the gamma-ray emission in panel (**B**) supports a hadronic origin in which molecular gas along the Galactic plane provides the dominant pp interaction target for Galactic cosmic rays. Reprinted with permission from Ref [13], Copyright 2026, Science.

The measured flux is a factor of ∼2 above the predictions of standard GALPROP-based CR propagation models that consider only diffuse hadronic emission [56,61]. This discrepancy deserves careful scrutiny given its potential significance: at face value, it represents a $\sim 2\sigma$-level tension between the data and the reference model, since the IceCube analysis quotes a flux normalization uncertainty of roughly 30–40% in the π^0 template fit [13], placing the factor-of-two excess at moderate but not yet decisive statistical significance. At the same time, the GALPROP predictions carry substantial systematic uncertainties of their own, arising from the adopted interstellar radiation field, the diffusion and re-acceleration parameter set, the assumed source distribution, and, critically, the gas column density templates used to compute the pp-interaction rate [58,61,62]. Variations in these inputs can shift the predicted neutrino flux by factors of 1.5–2 without violating existing observational constraints [57,58]. The discrepancy is therefore compatible with modeling limitations rather than constituting unambiguous evidence for new physics, but it is robust in the sense that it persists across the three spatial templates tested by IceCube and across independent analyzes [13,55].

On the physical interpretation side, several non-exclusive scenarios can account for the excess. First, the inner Galaxy may harbour a population of unresolved hadronic emitters, young massive star clusters, SNR–cloud interaction systems, and GMC complexes illuminated by nearby PeVatrons, whose integrated emission is not captured by the smooth GALPROP template [14]. Second, the CR spectral index in the inner few kpc may be harder than the local value assumed in standard propagation, perhaps due to the higher SNR density or to convective winds driven by the Galactic bar, leading to an enhanced pion-production rate per unit gas mass [57,63]. Third, the contribution of unresolved young massive stellar clusters (YMSCs), now recognized as efficient CR accelerators [64,65], may add a hadronic component on scales below the IceCube angular resolution that is not represented in the π^0 template. The factor-of-two excess could therefore be interpreted as a first indication that the inner Galaxy contains a richer population of hadronic PeVatrons than captured by current propagation models, potentially constituting a "smoking gun" for this enhanced source population once the statistical significance is increased by IceCube-Gen2 and KM3NeT/ARCA [66,67].

4.2. Neutrino Flux from Giant Molecular Cloud Populations

A systematic study of the collective neutrino output of cataloged GMC populations in the Galactic plane was performed by Roy et al. [14], who computed diffuse gamma-ray and neutrino fluxes under two scenarios for the Galactic CR distribution: (I) a spatially constant CR energy density and (II) a space-dependent CR distribution tracing the supernova rate. Under scenario I, the stacked neutrino flux from the full GMCs population falls about an order of magnitude below the IceCube π^0-template flux at 10^5 GeV. Under scenario II, the flux from GMCs in the innermost kpc ring around the Galactic Center rises to within a factor of a few of the IceCube sensitivity limit, owing to the strong CR enhancement toward the center implied by the SNR source distribution [14]. The spatial density distribution of GMC neutrino emitters in the latter scenario shows a clear concentration toward the Galactic Center and the Galactic Rift, both of which overlap with regions of enhanced significance in the IceCube significance map, providing a qualitative but suggestive correlation [14].

The study further showed that GMCs in the Galactic Rift region are particularly favorable targets for IceCube-Gen2, owing to their proximity, large molecular masses, and location near the horizon for the South Pole detector [14]. Taken together, the Roy et al. results establish that GMC populations can plausibly contribute a fraction of the observed IceCube Galactic plane flux, but are unlikely to account for the entire signal under conservative CR density assumptions, implying that additional source classes or enhanced inner-Galaxy CR densities are required.

4.3. The Gamma-Ray – Neutrino Multimessenger Balance

A central diagnostic for the hadronic fraction of the Galactic diffuse emission is the comparison of the measured gamma-ray and neutrino intensities in the same sky region. For a purely hadronic emitter, the relation given in Equation (8) predicts an accompanying gamma-ray flux that must be consistent with the total observed gamma-ray background. Fang et al. [55] showed that the pionic gamma-ray flux implied by the IceCube π^0-template best-fit is fully consistent with the Galactic diffuse gamma-ray emission measured by Fermi-LAT from 1 GeV to ∼1 TeV and by Tibet ASγ at ∼0.5 PeV, suggesting that the Galactic plane emission above ∼1 TeV is dominated by hadronic interactions rather than inverse Compton scattering or bremsstrahlung from electrons [13,55].

This conclusion has important implications for molecular clouds specifically. Gamma-ray observations by LHAASO have identified a sub-PeV diffuse component concentrated in the inner Galactic plane, whose intensity is broadly compatible with the IceCube flux when converted through Equation (8) [10]. Since the bulk of this sub-PeV gamma-ray emission is spatially correlated with the distribution of molecular gas in the inner Galaxy, the implication is that molecular clouds, as the densest and most abundant repositories of interstellar protons, dominate the hadronic calorimetric budget of the Galactic plane at TeV-PeV energies. The density contrast between the dense molecular phase ($n \sim 10^2$-10^3 cm^{-3}) and the warm intercloud medium ($n \sim 1$ cm^{-3}) means that the per-volume *pp* interaction rate is two to three orders of magnitude higher inside GMCs, so that despite occupying only a small volume fraction of the ISM, they are expected to dominate the total hadronic interaction rate along lines of sight near the Galactic plane [29]. We note, however, that the precise fraction, often quoted as $\gtrsim 70\%$, is model-dependent, relying on assumptions about the gas phase filling factors, the CO-to-H_2 conversion factor $X_{\rm CO}$, and the penetration depth of CRs into dense clumps [32]. In particular, if a significant fraction of the molecular gas is "CO-dark" H_2 not traced by standard CO surveys, the true contribution of dense gas to the interaction rate could be revised.

4.4. Searches for Individual Molecular Cloud Neutrino Sources

While the diffuse plane detection establishes that Galactic hadronic interactions produce high-energy neutrinos, no individual molecular cloud complex has yet been identified as a neutrino point or extended source. The IceCube Collaboration performed a dedicated search for extended neutrino emission from Galactic regions using ten years of muon-track data [68]. The most significant location in the scan, at 2.6σ post-trials, is a 1.7° region coincident with the unidentified TeV source 3HWC J1951+266, but no compelling association with a specific molecular cloud has been established [68].

The Cygnus region is among the most intensively studied northern-sky targets [69–72]. Using ten years of track events, IceCube searched for neutrino signals with four spatial templates (CO map, H I map, uniform disk, and 2D Gaussian), finding no significant emission [60]. The resulting 90% C.L. upper limit on the CO-template flux is

$$\frac{\mathrm{d}\Phi_\nu}{\mathrm{d}E_\nu} \leq 6.25 \times 10^{-17} \left(\frac{E_\nu}{100\,\mathrm{TeV}}\right)^{-3} \mathrm{TeV}^{-1}\,\mathrm{cm}^{-2}\,\mathrm{s}^{-1}, \tag{9}$$

which already constrains the hadronic fraction of the Cygnus Cocoon emission and disfavors models in which the

entire LHAASO Cygnus bubble flux is of hadronic origin [10,60].

For the SNR–cloud systems IC 443 and W 44, whose hadronic gamma-ray luminosities are well characterized ($L_\gamma \sim 10^{35}$–10^{36} erg s^{-1} [27]), the implied ν_μ flux at Earth via Equation (8) lies between $E_\nu^2 \Phi_{\nu_\mu} \sim 10^{-13}$ and 10^{-12} TeV cm^{-2} s^{-1}, one to two orders of magnitude below current IceCube point-source sensitivity. These systems, therefore, serve as reliable hadronic benchmarks but await next-generation instrumentation for individual detection.

Figure 5 illustrates the current IceCube point-source sensitivity alongside the predicted neutrino fluxes for representative molecular cloud systems, demonstrating the gap that future detectors must close. The LHAASO sources without associated pulsars, including LHAASO J2108+5157 and the extended Cygnus bubble emission, approach the sensitivity curve most closely and are prime candidates for follow-up neutrino searches [10,11].

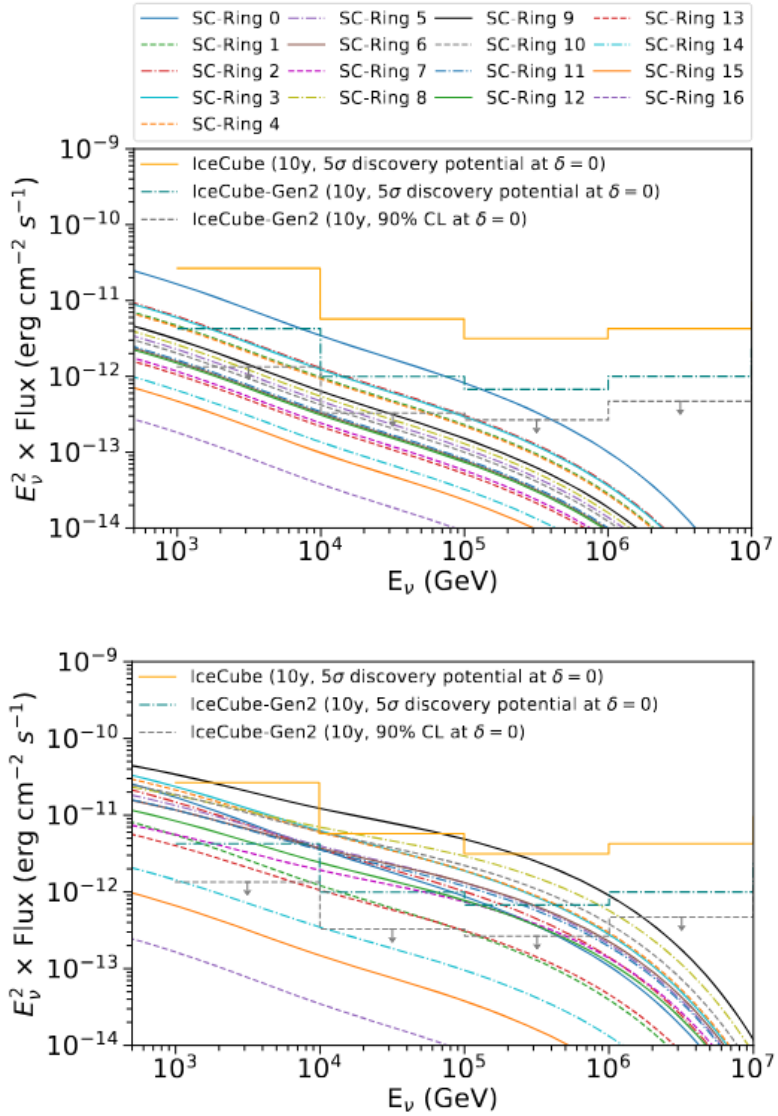

Figure 5. Predicted $\nu_\mu + \bar{\nu}_\mu$ energy fluxes from GMC populations compared with current and future detector sensitivities. Each curve corresponds to the stacked neutrino flux from GMCs located in a concentric 1 kpc-wide ring around the Sun (SC-Ring N, with Ring 0 centred on the solar neighbourhood and Ring 16 closest to the Galactic Centre). **Top panel:** constant Galactic CR flux (Case I); the maximum emission comes from the nearest ring, reflecting the dominance of close, well-catalogued GMCs. **Bottom panel:** radially varying CR flux following the supernova source distribution of [14] (Case IIb); the highest neutrino output shifts to the innermost Galactic ring, driven by the strong CR enhancement toward the Galactic Centre. In both panels, the orange horizontal line is the IceCube 10-year 5σ discovery potential at declination $\delta = 0°$; the cyan solid and dashed lines are the IceCube-Gen2 10-year 5σ discovery potential and 90% C.L. sensitivity, respectively. Under Case IIb, the innermost rings approach the current IceCube threshold, and the Galactic Rift region becomes detectable by IceCube-Gen2 within a decade of operation. Reprinted from Roy et al. [14].

4.5. Future Neutrino Telescope Prospects

The combination of next-generation neutrino telescopes offers complementary sky coverage and improved sensitivity that will transform the prospects for individual GMC detection over the next decade. Three instruments stand out as particularly relevant for the molecular cloud science case.

IceCube-Gen2 is the planned extension of the IceCube Neutrino Observatory at the South Pole, adding approximately 120 new detection strings to the existing 86 and increasing the instrumented volume to $\sim$8 km^3 [73]. The larger effective area translates into a factor-of-five improvement in point-source sensitivity relative to the current IceCube, lowering the detectable flux threshold to $E_\nu^2\Phi \sim \text{few} \times 10^{-13}$ TeV cm^{-2} s^{-1} for northern-sky sources with hard hadronic spectra, precisely the spectral shape expected from GMCs illuminated by PeVatron-escaped particles. At this sensitivity level, the brightest predicted GMC neutrino emitters in the Cygnus region and the Galactic Rift become detectable within a few years of operation [14,73].

In the Mediterranean, KM3NeT/ARCA is being deployed at 3500 m depth offshore Capo Passero, Sicily, with the full detector instrumenting $\sim$1 km^3 of seawater [67]. The low optical diffusion of seawater enables a muon-track angular resolution below 0.1° [67], which is superior to IceCube at comparable energies. The Northern Hemisphere location provides upgoing-neutrino visibility over 87% of the sky, including the Galactic Center and the majority of the inner Galactic plane, the sky region of maximum expected GMC hadronic output. Simulations of the full ARCA detector predict a 5σ detection of the diffuse astrophysical neutrino flux within half a year of operation, and the point-source sensitivity will surpass existing IceCube limits across the full sky [67]. Crucially, the Southern-sky coverage of KM3NeT/ARCA is complementary to IceCube: for Galactic sources such as W 28, the Central Molecular Zone, and the dense molecular complexes of the Norma–Scutum arm, ARCA will provide deeper sensitivity than any South-Pole-based instrument [74].

A third Northern Hemisphere instrument, the Baikal Gigaton Volume Detector (Baikal-GVD), operates in Lake Baikal at depths of 750–1300 m and extends the global neutrino telescope network with sensitivity to the 1–100 TeV range relevant for Galactic hadronic sources [75,76]. While its current angular resolution is inferior to KM3NeT/ARCA, Baikal-GVD contributes to full-sky coverage and provides independent cross-checks for candidate Galactic neutrino sources identified by IceCube and KM3NeT [75].

Taken together, the synergy between IceCube-Gen2, KM3NeT/ARCA, and Baikal-GVD, combined with gamma-ray constraints from CTAO and SWGO on the hadronic fraction in the Southern sky, constitutes a multimessenger program that, for the first time, makes the individual detection of GMC complexes as neutrino sources a realistic scientific objective within the coming decade.

5. Illuminated-Cloud Scenarios: Individual Source Case Studies

The physical framework developed in Sections 2–4 finds its most concrete expression in a handful of well-studied molecular cloud complexes, where multiwavelength data constrain the CR spectrum, the diffusion coefficient, and the target column density simultaneously. In each case, the cloud acts as a hadronic calorimeter, converting a fraction of the kinetic energy of nearby or escaping accelerators into gamma-ray and neutrino radiation. This section reviews the four systems that currently provide the most stringent multimessenger constraints: the W51 complex, the Cygnus X superbubble, the Central Molecular Zone, and the orphan UHE source LHAASO J2108+5157.

5.1. The W51 Complex

The W51 complex, located at $d \approx 5.5$ kpc in the Sagittarius arm, is one of the most massive and active star-forming regions in the Milky Way [77,78], and one of the few systems where hadronic acceleration has been confirmed at both GeV and sub-PeV energies [12,52,53]. The complex comprises the giant H II region W51A, the star-forming molecular cloud W51B, and the middle-aged supernova remnant W51C [78]. The interaction between the expanding shock of W51C and the dense molecular gas of W51B provides the physical setting for CR acceleration and subsequent hadronic emission [79,80].

At GeV energies, Fermi-LAT detected a clear spectral break near $\sim$200 MeV, consistent with the pion-decay kinematic threshold, establishing the hadronic nature of the emission without ambiguity [27]. The H.E.S.S. telescope subsequently detected the source at TeV energies, confirming a broadband hadronic spectrum extending from hundreds of MeV to tens of TeV [38]. The most recent and constraining measurement comes from LHAASO, which reported significant detection of gamma-ray emission from the W51 complex spanning 2 to 200 TeV [12]. For the first time, LHAASO extended the W51C gamma-ray spectrum beyond 100 TeV at more than 3σ significance and identified a pronounced spectral bending at tens of TeV, deviating from a pure power law [12]. The broadband spectrum from Fermi-LAT through LHAASO, spanning six decades in energy, can be self-consistently described by a single *pp*-collision hadronic model, providing compelling evidence that the radiation originates from collisions

between accelerated CRs and the dense molecular gas of W51B [12].

As shown in Figure 6, the spectral bending observed by LHAASO implies either an exponential cutoff at $E_p^{\rm cut} \approx 400$ TeV or a broken power law with a break near ∼200 TeV in the parent proton spectrum, making W51C the first evidence of a SNR serving as a CR accelerator approaching, though not yet reaching, the PeV regime [12]. An alternative scenario in which the UHE emission is powered by one of two young embedded star clusters within W51B (G48.9−0.3 or G49.2−0.3) cannot be excluded, as wind-termination shock scenarios within these clusters could also produce protons approaching PeV energies [12]. From the gamma-ray luminosity $L_\gamma \sim 10^{36}$ erg s^{-1} and the target proton column density inferred from CO and H I observations, the total energy in accelerated protons is estimated at $W_p \sim 10^{49}$–10^{50} erg, consistent with a fraction of order 1–10% of a canonical supernova explosion energy deposited in the adjacent molecular gas [12,38].

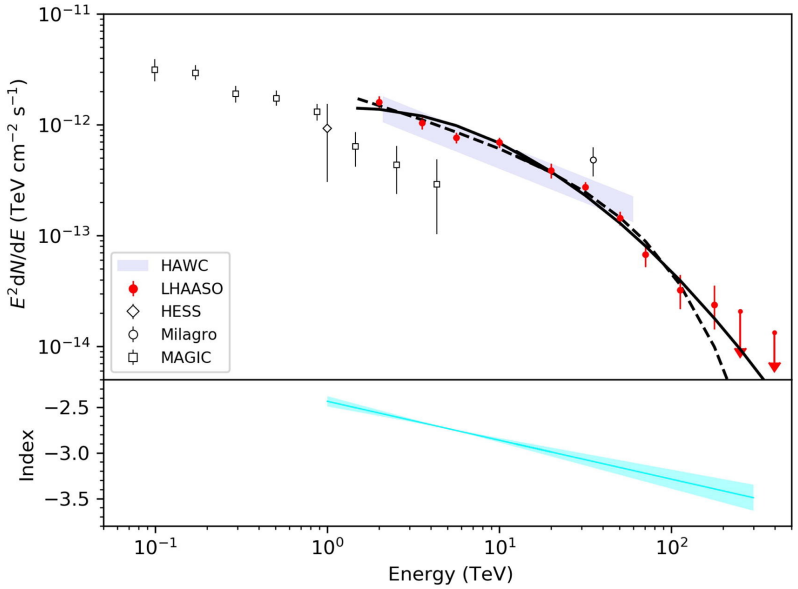

Figure 6. Spectral energy distribution of W51C plotted as $E^2\,\mathrm{d}N_\gamma/\mathrm{d}E_\gamma$. **Top panel:** Red filled diamonds are the LHAASO flux measurements covering $2.24^{+3.01}_{-1.28}$ to $177.83^{+46.04}_{-36.57}$ TeV, derived from a 3D likelihood analysis assuming a PLExpCut spectral model. Error bars are 1σ. Previous measurements from MAGIC, H.E.S.S., Milagro, and HAWC (shaded band) are shown for comparison, demonstrating the smooth spectral connection between the VHE and UHE regimes. The solid black line is the best-fit LOG (log-parabola) model; the dashed black line is the best-fit PLExpCut model. Both fits are consistent with a proton cutoff energy of $E_p^{\rm cut} \approx 400$ TeV, providing the first evidence for a SNR approaching the PeV acceleration regime. **Bottom panel:** Energy-dependent photon index $\Gamma(E)$ as derived from the LOG model fit; the cyan band represents the 1σ confidence interval. Reprinted with permission from Ref [12], Copyright 2026, Elsevier.

5.2. The Cygnus X Superbubble

The Cygnus X region at $d \approx 1.4$ kpc is the richest star-forming complex in the northern Galactic plane and arguably the most informative multimessenger laboratory currently available [81,82]. It harbors one of the most massive OB associations in the Galaxy (Cygnus OB2, containing ∼65 O-type stars), extensive molecular cloud complexes with a total mass of $\sim 3 \times 10^6\ M_\odot$ [81,83], and a spectacular γ-ray superbubble inflated by the collective stellar winds [69]. The multimessenger history of this region spans three distinct epochs of discovery.

The first epoch began when Fermi-LAT detected a 50-pc-wide cocoon of freshly accelerated CRs flooding the cavities carved by stellar winds and ionization fronts from the young clusters in Cygnus X [69]. The Cygnus Cocoon, as it became known, showed a hard spectrum ($\Gamma \approx 2.0$) at 1–100 GeV, inconsistent with the local CR sea and indicative of particles accelerated within the last few thousand years before interacting with the surrounding molecular gas. HAWC subsequently confirmed TeV emission from the Cocoon region at 1–100 TeV with spectral softening to $\Gamma \approx 2.6$, consistent with CR leakage from the acceleration region into the surrounding interstellar medium [10].

The second epoch arrived with the LHAASO discovery of an enormous γ-ray bubble spanning at least $100\,\mathrm{deg}^2$ toward the Cygnus X region at UHE, with eight photons above 1 PeV detected, including one at 2.5 PeV [72]. The bubble spectrum follows a log-parabola form with $\Gamma(E) = (2.71 \pm 0.02) + (0.11 \pm 0.02) \times \log_{10}(E/10\,\mathrm{TeV})$ over the full 2 TeV–2 PeV range [72]. Within the bubble, LHAASO identified UHE hotspots spatially correlated with the most massive molecular cloud complexes, a direct signature of the illuminated-cloud scenario in which

PeVatron-escaped particles are reprocessed into gamma rays and neutrinos by dense hadronic targets. The intensity of the UHE emission is clearly correlated with the distribution of the surrounding molecular gas, and Cygnus OB2, in the core of the bubble, is the leading candidate for the super-PeVatron accelerating CRs to at least 10 PeV [72].

As shown in Figure 7, the spatial morphology of the Cygnus bubble evolves systematically across three decades of photon energy. At 2–20 TeV, the emission is dominated by the bright central core associated with the Cygnus OB2 region, while at 25–100 TeV, the structure begins to reveal the extended bubble, with peripheral hotspots emerging above the diffuse background [72]. Above 100 TeV, the hotspots become the defining morphological feature and are spatially correlated with the local molecular cloud distribution, as indicated by the white contours tracing the CO gas [72]. This energy-dependent morphology is a direct signature of the illuminated-cloud scenario: the highest-energy particles preferentially illuminate the densest molecular targets nearest to the acceleration region, while lower-energy particles fill a more extended diffuse halo. The one-dimensional flux profiles along Galactic longitude confirm that the molecular gas column density, rather than the radiation or magnetic field geometry, controls the spatial distribution of the UHE emission, with the inner and outer Galaxy gas components contributing distinctly at the highest energies [72]. The overall broadband spectrum from 1 GeV to 2 PeV is reproduced by a hadronic model in which protons are continuously injected at the core and diffuse outward to at least 150 pc, with a diffusion coefficient $D \sim 10^{28}$–10^{29} cm^2 s^{-1} appropriate for the turbulent superbubble environment [72]. The leptonic origin of the PeV photons is strongly disfavored: 100-TeV electrons suffer severe synchrotron and inverse Compton losses in the intense magnetic and radiation fields of Cygnus X, confining them to distances far smaller than the observed bubble extent, whereas PeV protons propagate freely to the peripheral molecular clouds where they produce the observed UHE hotspots.

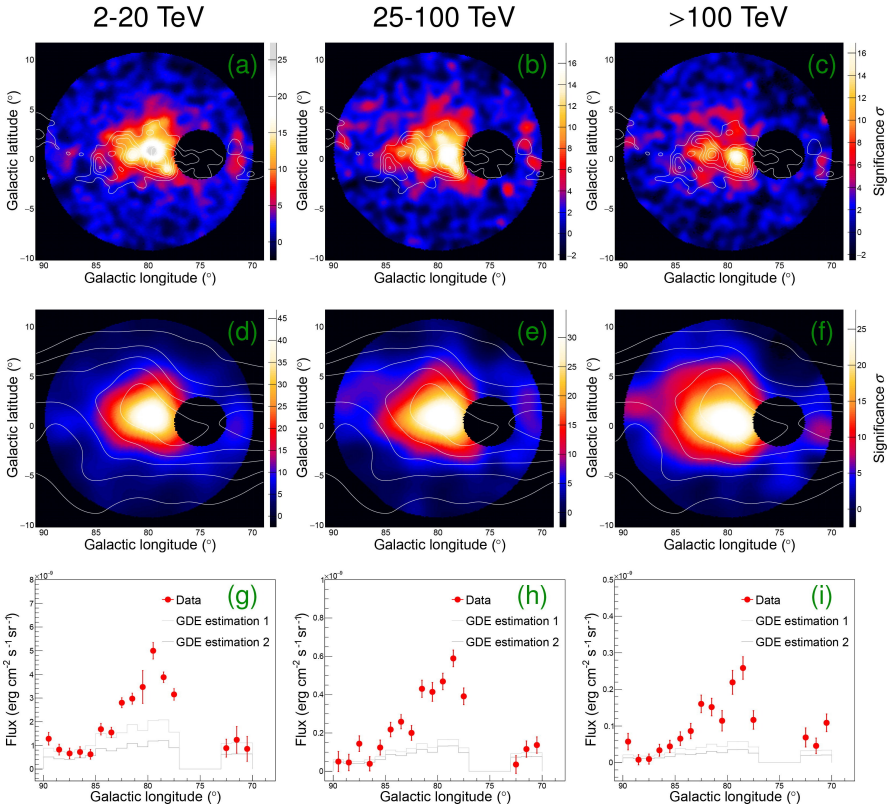

Figure 7. The Cygnus γ-ray bubble across three decades of photon energy. **Top two rows:** Two-dimensional significance maps of the bubble in the ranges 2–20 TeV (left), 25–100 TeV (centre), and >100 TeV (right), smoothed with a Gaussian kernel of $\sigma = 0.3^\circ$ (upper row) and $\sigma = 1^\circ$ (middle row); all individual sources including SNR γ-Cygni are removed. White contours trace the local molecular cloud distribution from CO observations. Hotspots correlated with the molecular gas are revealed at energies above 25 TeV and become the dominant morphological feature above 100 TeV, a direct signature of the illuminated-cloud scenario in which PeVatron-escaped protons interact with dense molecular targets. **Bottom row:** One-dimensional γ-ray flux profiles along Galactic longitude in the latitude range -2° to 2°; GDE estimation 1 and estimation 2 represent contributions from the inner and outer Galaxy gas components separately. The energy-dependent morphology and the gas-correlated UHE hotspots are consistent with a hadronic model in which protons are continuously injected by the Cygnus OB2 super-PeVatron and diffuse outward through the circumstellar molecular gas. Reprinted with permission from Ref [72], Copyright 2026, Elsevier.

From the neutrino side, IceCube performed a dedicated template search for emission from the Cygnus Bubble using seven years of muon-track data, testing four spatial templates, including the CO molecular cloud map and the H I gas map [84]. No significant signal was found, but the resulting upper limits on the CO-template neutrino flux already constrain the hadronic fraction of the bubble emission and are approaching the level where next-generation instruments will provide definitive tests of the super-PeVatron hypothesis [60,84].

5.3. The Central Molecular Zone

The Central Molecular Zone (CMZ), the ∼200-pc ring of dense molecular gas surrounding the Galactic Center, represents the most extreme hadronic interaction environment in the Galaxy [85,86]. With a total molecular mass of $\sim 5 \times 10^7\, M_\odot$, typical gas densities of $n \sim 10^3$–$10^4\,\mathrm{cm}^{-3}$ [86], and CR energy densities an order of magnitude above the local solar neighborhood value [87], the CMZ is simultaneously the most massive hadronic target and the most CR-intense region accessible to gamma-ray telescopes.

H.E.S.S. observations of the inner 300 pc established the foundational picture of the CMZ as a multimessenger source [87]. The diffuse VHE γ-ray emission detected along the Galactic ridge is strongly correlated with the molecular gas distribution as traced by CS line emission, and the inferred CR energy density follows an approximately $1/r$ radial profile consistent with continuous injection from a central source, most plausibly associated with the supermassive black hole Sgr A* or the young massive star clusters (Arches, Quintuplet, and Nuclear Star Cluster) within the inner few parsecs [87]. The gamma-ray spectrum follows a hard power law with $\Gamma \approx 2.3$ extending to tens of TeV without a statistically significant cutoff, implying a parent proton spectrum reaching close to 1 PeV and establishing the Galactic Center as the first robust detection of a Galactic PeVatron [87].

More recent work has refined this picture significantly. Scherer & Cuadra [88] developed CR transport models with two distinct diffusion regimes (inside and outside the CMZ) plus polar advection, reproducing both the VHE (1–100 TeV) and HE (10–300 GeV) gamma-ray morphology simultaneously within a unified scenario in which CRs are accelerated from the Nuclear Star Cluster, Wolf-Rayet stellar winds, and the young supernova remnant Sgr A East. In their model, the diffusion coefficient inside the CMZ is suppressed to $D_{\mathrm{CMZ}} \sim 10^{26}\,\mathrm{cm}^2\,\mathrm{s}^{-1}$, two orders of magnitude below the standard Galactic value, consistent with the high level of turbulence inferred from molecular line observations of the dense gas [88]. The suppressed diffusion is critical for the multimessenger output: it confines CRs within the CMZ long enough to interact efficiently with the molecular gas, maintaining a high hadronic emissivity throughout the $\sim 5 \times 10^7\, M_\odot$ molecular reservoir.

The predicted neutrino flux from the CMZ, derived via Equation (8) from the H.E.S.S. gamma-ray measurements, is $E_\nu^2 \Phi_{\nu_\mu} \sim 10^{-12}\,\mathrm{TeV\,cm^{-2}\,s^{-1}}$ at ∼10 TeV, tantalizingly close to current detection thresholds [74,89]. The southern-sky location of the Galactic Center ($\delta \approx -29^\circ$) places it in the IceCube cascade-dominated regime with limited angular resolution, but within the optimal field of view of KM3NeT/ARCA, for which the CMZ is one of the highest-priority Galactic neutrino targets [74]. The CTAO Galactic Center Key Science Project will provide a definitive measurement of the CMZ gamma-ray morphology and spectrum at sub-arcminute resolution across 0.1–100 TeV, directly constraining the CR injection rate and the PeVatron identification [17].

5.4. LHAASO J2108+5157: An Orphan Illuminated Cloud

Among the LHAASO UHE sources, LHAASO J2108+5157 occupies a special place in the illuminated-cloud scenario because it has no known conventional counterpart, no SNR, no pulsar wind nebula, and no active star-forming region within its localization region [10]. Its UHE emission therefore cannot be attributed to particle acceleration within the source itself, and the most natural interpretation is the illuminated-cloud scenario: a nearby but as-yet-unidentified PeVatron has injected CRs that are being reprocessed into gamma rays by interaction with a molecular cloud that happens to lie in the path of the escaping particle flux [11].

Mitchell [11] performed a dedicated hadronic modeling study of LHAASO J2108+5157 as a molecular cloud illuminated by a SNR. The analysis showed that the observed UHE flux requires a young SNR (< 10 kyr old) located within 40–60 pc of the cloud, with a maximum proton energy of ∼3 PeV and a low Sedov parameter, ensuring that the bulk of the CR energy is still confined near the remnant and has not yet diffused away [11]. The Galactic CR sea alone is insufficient to account for the observed flux, so an additional local PeVatron must be present. No SNR matching these properties is currently known in the region, although an undetected remnant remains entirely feasible given the incompleteness of current Galactic SNR catalogs at large distances [11]. The required local diffusion coefficient at the cloud is $D_{\mathrm{cloud}} \sim 10^{25}$–$10^{26}\,\mathrm{cm}^2\,\mathrm{s}^{-1}$, significantly below the standard Galactic value and consistent with CR self-confinement near the acceleration region [11,15,38,90].

The LHAASO J2108+5157 system is particularly valuable as a test case because its lack of a known counterpart makes it uniquely dependent on multimessenger observations for physical interpretation. Its predicted ν_μ flux at

Earth via Equation (8) lies at $E_\nu^2 \Phi_{\nu_\mu} \sim 10^{-13}\,\mathrm{TeV\,cm^{-2}\,s^{-1}}$, below current IceCube sensitivity but within the projected reach of IceCube-Gen2 for a hard-spectrum northern-sky source [14,73]. A neutrino detection coincident with this source would simultaneously confirm the hadronic origin of its UHE emission and provide the first identification of a PeVatron through its neutrino signal rather than through its gamma-ray morphology.

Taken together, the four systems reviewed in this section illustrate the diversity of physical configurations through which molecular clouds become multimessenger sources: direct SNR-cloud interaction in W51, superbubble illumination in Cygnus X, continuous PeVatron injection into a circumnuclear molecular reservoir in the CMZ, and orphan cloud illumination in LHAASO J2108+5157. In each case, the cloud acts as the hadronic interaction target, in the thin-target limit for less dense or more extended clouds, or approaching calorimetric behaviour for the densest systems, and the gamma-ray spectrum encodes the spectrum of the illuminating proton population modulated by the transport properties within the cloud. The neutrino flux predicted by Equation (8) is within a factor of a few of the sensitivity of next-generation detectors for all four systems, making the coming decade the decisive epoch for multimessenger molecular cloud astronomy.

6. Future Prospects

The coming decade will transform our understanding of molecular clouds as multimessenger sources through a new generation of observatories operating across the electromagnetic spectrum and in the neutrino channel. The complementarity between these facilities is essential: gamma-ray observatories will pin down the hadronic spectral signatures and spatial morphology of CR interactions in molecular gas, while neutrino telescopes will provide the smoking-gun confirmation of the hadronic origin that gamma rays alone cannot deliver.

6.1. Gamma-Ray Observatories

CTAO, now formally established as a European Research Infrastructure Consortium, will represent a qualitative leap in VHE gamma-ray astronomy, with a factor of five to ten improvement in sensitivity over current IACTs across the energy range from a few tens of GeV to beyond 300 TeV [17]. Its angular resolution of $\lesssim 0.05^\circ$ above 1 TeV [17] will resolve the internal structure of nearby molecular complexes such as the Cygnus superbubble and the W51 region [91], enabling direct mapping of the CR density profile within the clouds and a precise determination of the diffusion coefficient as a function of position [17,92]. Crucially, CTAO will also be able to distinguish the nuclear composition of the parent CRs from the spectral shape of the hadronic gamma-ray emission alone: simulations for SNR-cloud systems such as RX J1713.7−3946 and HAWC J2227+610 show that CTAO will discriminate between proton- and heavy-nucleus-dominated scenarios and constrain the spectral cutoff sharpness β to values inaccessible with current instruments [93]. This capability is directly applicable to illuminated molecular clouds, where the nuclear composition of runaway CRs carries information about the acceleration history and the magnetic rigidity of the confining fields near the source.

The southern array, located at the Cerro Armazones site near the ESO Paranal Observatory in the Atacama Desert, Chile, at an altitude of approximately 2600 m a.s.l. [17], is optimally placed to survey the Galactic center region and the Central Molecular Zone, where the H.E.S.S. detection of a $1/r$ CR gradient has established the Galactic center as the prime PeVatron candidate [87]. The CTAO Galactic Center Key Science Project will measure the spectrum of the diffuse VHE emission to energies well above 100 TeV, directly testing whether the accelerator sustains a PeV proton spectrum at the present epoch and constraining the age and power of the central source [17]. For the W51 complex specifically, dedicated CTAO simulations of the SNR–MC interaction region demonstrate that combining CTAO with the ASTRI Mini-Array will bridge the critical 0.3–100 TeV spectral gap between Fermi-LAT and LHAASO, resolving the spectral break that distinguishes a true PeVatron cutoff from a change in the target gas density [91].

For passive molecular clouds acting as CR barometers, CTAO will extend the pion-bump measurement to a statistically significant sample of SNR-cloud associations across the Galaxy, building on the pioneering Fermi-LAT detections of IC 443 and W44 [27]. The combination of CTAO with Fermi-LAT data will provide continuous spectral coverage from ∼100 MeV to ∼300 TeV, allowing for a robust separation of the hadronic and leptonic components and a precise measurement of the proton spectral index in diverse environments. Crucially, CTAO will probe the spectral cutoff region in illuminated clouds such as W51 and the CMZ, directly constraining the maximum energy of the parent proton population and thus the nature of the PeVatron [12,87].

SWGO, whose site has been selected at the Atacama Astronomical Park in Chile at an altitude of >4400 m, will provide continuous all-sky monitoring from ∼300 GeV to beyond 1 PeV [22]. Its graded-zone design, combining a dense inner array of dual-layer water Cherenkov detectors with a sparser outer array covering up to $2\,\mathrm{km}^2$, yields efficient gamma-ray detection from 300 GeV to PeV energies, surpassing LHAASO KM2A at the highest energies

and extending the sensitivity of the HAWC Observatory with a significantly lower energy threshold due to its high-altitude location [22]. Like LHAASO in the northern hemisphere, SWGO will survey the entire southern sky without scheduling constraints, making it uniquely suited to detect extended and time-variable UHE emission from molecular cloud complexes in the inner Galaxy. At TeV energies, SWGO will have the capacity to detect diffuse emission at the scale of molecular clouds, down to 0.1°–3° in the inner Galaxy, analogous to what Fermi-LAT has achieved at GeV energies [22]. Its wide field of view will be indispensable for characterizing the large-scale morphology of superbubbles, such as the Cygnus X region, and for searching for new illuminated-cloud systems in the southern Galactic plane, complementing the LHAASO first catalog [10] with equivalent southern coverage. Simulations show that SWGO could significantly detect nearby molecular cloud systems up to 300 TeV and could discriminate between interstellar emission models featuring different CR transport properties even above 50 TeV [22]. The combination of SWGO and CTAO will provide both the sensitivity for faint extended sources and the angular resolution required to resolve their internal structure.

6.2. Neutrino Telescopes

The detection of Galactic plane neutrino emission by IceCube at 4.5σ significance [13] has opened the era of Galactic neutrino astronomy, but the identification of the individual molecular cloud complexes responsible for that emission requires the next generation of neutrino telescopes. IceCube-Gen2, the proposed extension of the IceCube detector to approximately $8\,\mathrm{km}^3$ of instrumented volume through the addition of 120 new strings deployed at 240 m spacing, will deliver a factor of five improvement in point-source sensitivity and more than double the muon track lengths for improved angular resolution [66]. This gain translates directly into the ability to detect the stacked neutrino signal from the GMC population in the inner Galaxy, particularly the SC-Ring component identified by Roy et al. [14], whose predicted flux in the Case-IIb (SNR-dependent CR) scenario approaches the current IceCube threshold. The Aquila Rift complex, which Roy et al. identify as especially neutrino-bright and favorable for IceCube-Gen2 detection [14], is also included. IceCube-Gen2 will also extend the measurable energy range toward multi-PeV neutrinos [66,73,94], enabling a direct spectral comparison with the UHE gamma-ray observations from LHAASO and SWGO [22,94], thus providing a model-independent test of the hadronic hypothesis in individual source regions [95]. The IceCube-Gen2 surface array, with full efficiency for proton showers above 0.5 PeV and an aperture 30 times larger than IceCube, will additionally provide sensitivity to PeV gamma rays and cosmic-ray anisotropy measurements in the PeV range, directly probing the escape of CRs from Galactic PeVatrons such as the W51 and Cygnus systems [94].

KM3NeT/ARCA, deployed at 3500 m depth offshore Capo Passero, Sicily, provides critical complementarity to IceCube through its superior angular resolution ($< 0.1^\circ$ for muon-neutrino tracks at $\gtrsim 100$ TeV), its unobstructed view of the Galactic center and southern sky where IceCube's effective area is suppressed, and its 1 km^3 instrumented volume [67]. By leveraging both track and shower event topologies, KM3NeT/ARCA is projected to achieve a 5σ detection of the diffuse astrophysical neutrino flux within half a year of full operation and to resolve the morphological contribution of individual GMC complexes, including the CMZ, the Norma arm clouds, and the W51 region, within a few years [67]. The sensitivity to point-like sources across the entire sky surpasses existing observed limits, placing KM3NeT/ARCA in a unique position to constrain the neutrino flux from well-modeled hadronic sources such as the CMZ and the Cygnus Bubble, for which detailed hadronic predictions now exist [60,67]. The Central Molecular Zone is a particularly compelling target: the predicted ν_μ flux of $\sim 10^{-12}\,\mathrm{TeV\,cm^{-2}\,s^{-1}}$ at $\sim$10 TeV from hadronic interactions in the CMZ lies within the reach of KM3NeT/ARCA, and a detection would unambiguously confirm the hadronic PeVatron interpretation of the H.E.S.S. measurement [74]. In the northern sky, Baikal-GVD, currently expanding toward $\sim$1 km^3 in Lake Baikal [75], will contribute complementary sensitivity to Galactic sources at intermediate declinations, reinforcing the global neutrino coverage of the inner Galaxy [76].

6.3. Multimessenger Synergies

The full scientific return of the coming generation of facilities will be realized through joint multimessenger analyzes that combine the information content of gamma rays, neutrinos, and cosmic rays simultaneously. The gamma-ray/ν flux ratio is a powerful diagnostic: for a pure hadronic source, the ratio $E_\nu^2\Phi_{\nu_\mu+\bar{\nu}_\mu} \approx \frac{1}{2}E_\gamma^2\Phi_\gamma|_{E_\gamma=2E_\nu}$ is predicted with little theoretical uncertainty [24,25], so any significant deviation signals either a leptonic contamination of the gamma-ray flux or neutrino oscillation effects that must be modeled. Joint spectral fits combining CTAO, SWGO, and IceCube-Gen2 data will constrain the proton spectral index, the total CR energy budget, and the gas column density along the line of sight with unprecedented precision, effectively turning GMC complexes into precision laboratories for hadronic CR physics. This program is already being demonstrated in the current generation: the HAWC Galactic diffuse emission analysis, applying source-subtraction algorithms developed for the

CTAO Galactic Plane Survey [17,96], reveals significant residual emission beyond $|b| > 3^\circ$ correlated with Galactic gas [97], providing the TeV counterpart of the Fermi-LAT barometer measurements [45,46] and a direct benchmark for CTAO and SWGO.

From the cosmic-ray side, the Pierre Auger Observatory and its upgrade, AugerPrime [98], are measuring the nuclear composition of CRs in the EeV range with increasing precision, probing the transition from Galactic to extragalactic CRs and constraining the maximum energy delivered by Galactic PeVatrons, such as the Cygnus OB2 association [1]. Correlating the Auger anisotropy measurements with the spatial distribution of molecular cloud complexes and their associated UHE gamma-ray emission [72] will help identify the highest-energy end of the Galactic CR spectrum and clarify whether sources such as the Cygnus super-PeVatron can sustain acceleration to the knee and beyond.

Finally, the advent of high-resolution molecular line surveys, with facilities such as the Square Kilometer Array (SKA) and the next generation Very Large Array (ngVLA) [99], will provide the gas column density maps required to convert observed gamma-ray and neutrino fluxes into precise CR density measurements [100]. Accurate three-dimensional maps of the molecular gas distribution, combined with the gamma-ray emissivity profiles measured by CTAO and SWGO, will allow a tomographic reconstruction of the CR density field in the inner Galaxy, directly testing the predictions of CR transport models and revealing whether the interstellar CR spectrum is truly uniform or shows the source-to-source variations hinted at by current Fermi-LAT observations [101].

7. Summary and Conclusions

Molecular clouds have emerged as one of the most productive laboratories for hadronic cosmic-ray physics in the Galaxy. Their large gas column densities, well-characterized molecular line tracers, and proximity to known CR accelerators make them ideal targets for multimessenger observations spanning the GeV-to-PeV gamma-ray band and the TeV neutrino domain. In this review, we have examined the physical mechanisms, observational evidence, and theoretical modeling that underpin the use of GMCs as multimessenger sources, and we summarize the main conclusions below.

The hadronic interaction chain, proton-proton collisions producing charged and neutral pions that decay into neutrinos and gamma rays, respectively, is the physical foundation linking all three messenger channels. The *pp* interaction timescale $t_{pp} \approx 5.3 \times 10^7 (n/100\,\mathrm{cm}^{-3})^{-1}$ yr sets the efficiency of molecular clouds as CR calorimeters, and the nuclear enhancement factor $\kappa_{\rm nuc} \approx 1.5$–$1.8$ accounts for the contributions of heavier nuclei in both the CR beam and the target gas [24,25]. The parametric emissivity functions of Kelner et al. and Kafexhiu et al. now provide percent-level accuracy in translating a given proton spectrum into observable photon and neutrino fluxes, removing a major source of theoretical uncertainty from multimessenger predictions. CR transport within and around molecular clouds is governed by energy-dependent diffusion, with coefficients inside clouds ($D_{\rm cloud} \sim 10^{25}$–$10^{26}\,\mathrm{cm}^2\,\mathrm{s}^{-1}$) significantly suppressed relative to the interstellar average, a suppression that imprints characteristic spectral and morphological signatures on the gamma-ray emission that CTAO will measure with sufficient spatial resolution to map directly [17,28].

In the gamma-ray domain, the observational landscape has been transformed over the past fifteen years by three complementary facilities operating at different energies. Fermi-LAT established the hadronic origin of GeV emission from SNRs-cloud systems such as IC 443 and W44 through the unambiguous detection of the pion-decay spectral break, providing the first direct proof that SNRs accelerate CR protons [27]. It also revealed the radial gradient of the CR density in the inner Galaxy using passive molecular clouds as barometers, establishing that the interstellar CR spectrum is not uniform but rises toward the Galactic center [101]. At VHE energies, H.E.S.S. detected diffuse TeV emission from the Central Molecular Zone correlated with the dense gas distribution and exhibiting a $1/r$ CR density profile, providing the first robust observational evidence for a PeVatron at the Galactic center [87]. At UHE, LHAASO has opened an entirely new window: its first source catalog revealed PeV emission from numerous Galactic sources, several of which are spatially coincident with molecular cloud complexes [10]. The LHAASO observations of W51 detected photons above 100 TeV and established a proton cutoff energy of $E_p^{\rm cut} \approx 400$ TeV, with a total hadronic energy budget of $W_p \sim 10^{49}$–10^{50} erg [12]. The Cygnus Bubble, powered by the Cygnus OB2 super-PeVatron, showed energy-dependent morphology with UHE hotspots correlated with the molecular gas distribution, accelerating protons to energies of at least 10 PeV and exhibiting a diffusion coefficient $D \sim 10^{28}$–$10^{29}\,\mathrm{cm}^2\,\mathrm{s}^{-1}$ appropriate for a turbulent superbubble environment [72]. The orphan UHE source LHAASO J2108+5157, lacking any known counterpart, is best explained as a molecular cloud illuminated by a young, as-yet-unidentified SNR within 40–60 pc, requiring proton energies of $E_p^{\rm max} \sim 3$ PeV and a CR diffusion coefficient inside the cloud of $D_{\rm cloud} \sim 10^{25}$–$10^{26}\,\mathrm{cm}^2\,\mathrm{s}^{-1}$ [11].

In the neutrino channel, the IceCube detection of Galactic plane emission at 4.5σ significance, with the highest

significance template being the π^0 model correlated with the gas distribution, constitutes the first direct evidence that hadronic CR interactions contribute substantially to the diffuse Galactic neutrino background [13]. The observed flux exceeds GALPROP model expectations by a factor of $\sim$2; as discussed in Section 4.1, the statistical significance of this discrepancy is moderate ($\sim 2\sigma$ given the template normalization uncertainties), and systematic uncertainties in the propagation models are themselves comparable in magnitude [58,61,62]. The excess is nevertheless robust across all tested spatial templates and is consistent with either a harder inner-Galaxy CR spectral index [57,63] or an additional population of unresolved hadronic sources, including young massive stellar clusters [64,65] and GMC complexes illuminated by nearby PeVatrons [14], making it one of the most compelling targets for IceCube-Gen2 and KM3NeT/ARCA [66,67]. Population models of GMCs [14] demonstrate that molecular cloud complexes, particularly those in the inner Galaxy SC-Ring, can account for a significant fraction of this excess in scenarios where the CR luminosity scales with the local SNR distribution, approaching the IceCube detection threshold and pointing toward the Aquila Rift and Galactic Rift as the most favorable detection targets for next-generation instruments. No individual GMC has yet been detected as a neutrino point source, with the most significant excess reaching only 2.6σ in extended source searches [68], and IceCube upper limits on the Cygnus CO-template neutrino flux are now approaching the level predicted by hadronic models [60].

The illuminated-cloud scenario, in which runaway CRs that have escaped their acceleration site diffuse into a nearby molecular cloud and produce enhanced gamma-ray and neutrino emission, unifies the diverse observational phenomenology reviewed here. The four case studies examined, W51, the Cygnus Bubble, the Central Molecular Zone, and LHAASO J2108+5157, span a wide range of accelerator types (SNR, stellar wind superbubble, central massive black hole, unidentified), cloud environments (dense GMC, diffuse extended superbubble, extreme CMZ conditions), and CR energetics, yet all are naturally accommodated within this common framework. The common thread is that the molecular gas column density, rather than the radiation or magnetic field geometry, controls the spatial distribution and spectral normalization of the UHE emission, making CO and CS molecular line maps indispensable complements to gamma-ray and neutrino observations.

Looking forward, the convergence of CTAO, SWGO, IceCube-Gen2, and KM3NeT/ARCA will provide an order-of-magnitude leap in sensitivity across all three messenger channels simultaneously. CTAO will resolve the CR density profile within nearby molecular complexes and constrain the diffusion coefficient as a function of position, while SWGO will provide the wide-field UHE monitoring needed to discover new illuminated-cloud systems in the southern sky and characterize the large-scale CR distribution in the inner Galaxy [17,22]. IceCube-Gen2, with its factor-of-five sensitivity gain and extended energy reach into the multi-PeV domain, will either detect the predicted stacked neutrino signal from GMC populations or place constraints tight enough to rule out the hadronic interpretation of the IceCube Galactic plane excess [66]. KM3NeT/ARCA, with its sub-0.1° angular resolution and privileged view of the Galactic center, is projected to detect the diffuse Galactic plane neutrino flux at 5σ within its first year of full operation and to resolve the contribution of individual complexes, including the CMZ and W51, within a few years [67]. The joint analysis of gamma-ray and neutrino fluxes from the same molecular cloud systems, constrained by the theoretical prediction $E_\nu^2 \Phi_{\nu_\mu+\bar{\nu}_\mu} \approx \frac{1}{2} E_\gamma^2 \Phi_\gamma|_{E_\gamma = 2E_\nu}$ [24], will provide model-independent tests of the hadronic hypothesis and precision measurements of the proton spectral index in environments spanning four decades in gas density.

In summary, molecular clouds occupy a central and irreplaceable role in multimessenger astrophysics. As passive barometers, they record the integrated CR history of their environment; as active targets in the illuminated-cloud scenario, they amplify the gamma-ray and neutrino yields of nearby PeVatrons to detectable levels; and as the dominant hadronic target in the interstellar medium, they set the normalization of the diffuse Galactic neutrino background against which individual source contributions must be measured. The next decade of joint gamma-ray, neutrino, and molecular line observations will establish whether the Galactic CR spectrum is truly shaped by a handful of dominant PeVatrons or by a distributed population of moderate accelerators embedded in the molecular gas of the spiral arms, a question that lies at the heart of the century-old problem of the origin of cosmic rays.

Funding

This research was funded by the Fundação de Amparo à Pesquisa do Estado de São Paulo (FAPESP), grant numbers 2021/01089-1, 2024/02267-9, and 2024/14769-9, and by the Conselho Nacional de Desenvolvimento Científico e Tecnológico (CNPq), grant numbers 403337/2024-0, 153839/2024-4, and 200164/2025-2.

Institutional Review Board Statement

Not applicable.

Informed Consent Statement

Not applicable.

Data Availability Statement

Not applicable.

Conflicts of Interest

The author declares no conflict of interest.

Use of AI and AI-Assisted Technologies

During the preparation of this work, the author used the AI tool Claude (Anthropic) for grammar checking and language editing. After using this tool, the author carefully reviewed and revised all content as needed and take full responsibility for the final version of the published article.

References

1. Spurio, M. *Probes of Multimessenger Astrophysics: Charged Cosmic Rays, Neutrinos, γ-Rays and Gravitational Waves*, 2nd ed.; Springer: Cham, Switzerland, 2018.
2. Gabici, S.; Evoli, C.; Gaggero, D.; et al. The Origin of Galactic Cosmic Rays: Challenges to the Standard Paradigm. *Int. J. Mod. Phys. D* **2019**, *28*, 1930022.
3. Navas, S.; Amsler, C.; Gutsche, T.; et al. Review of Particle Physics. *Phys. Rev. D* **2024**, *110*, 030001.
4. Becker, J.K. High-Energy Neutrinos in the Context of Multimessenger Astrophysics. *Phys. Rep.* **2008**, *458*, 173–246.
5. Halzen, F.; Kheirandish, A. Multimessenger Search for the Sources of Cosmic Rays Using Cosmic Neutrinos. *Front. Astron. Space Sci.* **2019**, *6*, 32.
6. Ferrière, K.M. The Interstellar Environment of Our Galaxy. *Rev. Mod. Phys.* **2001**, *73*, 1031–1066.
7. Acero, F.; Ackermann, M.; Ajello, M.; et al. Development of the Model of Galactic Interstellar Emission for Standard Point-Source Analysis of Fermi Large Area Telescope Data. *Astrophys. J. Suppl.* **2016**, *223*, 26.
8. Mizuno, T.; Hayashi, K.; Metzger, J.; et al. Gas and Cosmic-Ray Properties in the MBM 53, 54, and 55 Molecular Clouds and the Pegasus Loops Revealed by H I Line Profiles, Dust, and Gamma-Ray Data. *Astrophys. J.* **2022**, *935*, 97.
9. Cao, Z.; Aharonian, F.A.; An Q.; et al. Ultrahigh-Energy Photons up to 1.4 Petaelectronvolts from 12 γ-Ray Galactic Sources. *Nature* **2021**, *594*, 33–36.
10. Cao, Z.; Aharonian, F.; An Q.; et al. The First LHAASO Catalog of Gamma-Ray Sources. *Astrophys. J. Suppl.* **2024**, *271*, 25.
11. Mitchell, A.M.W. LHAASO J2108+5157 as a Molecular Cloud Illuminated by a Supernova Remnant. *Astron. Astrophys.* **2024**, *684*, A66.
12. Cao, Z.; Aharonian, F.; Bai, Y.X.; et al. Evidence for Particle Acceleration Approaching PeV Energies in the W51 Complex. *Sci. Bull.* **2024**, *69*, 2833–2841.
13. Abbasi, R.; Ackermann, M.; Adams, J.; et al. Observation of High-Energy Neutrinos from the Galactic Plane. *Science* **2023**, *380*, 1338–1343.
14. Roy, A.; Joshi, J.C.; Cardillo, M.; et al. Gamma-Rays and Neutrinos from Giant Molecular Cloud Populations in the Galactic Plane. *J. Cosmol. Astropart. Phys.* **2024**, *2024*, 074.
15. Gabici, S.; Aharonian, F.A.; Casanova, S. Broad-Band Non-Thermal Emission from Molecular Clouds Illuminated by Cosmic Rays from Nearby Supernova Remnants. *Mon. Not. R. Astron. Soc.* **2009**, *396*, 1629–1639.
16. Aharonian, F.A.; Atoyan, A.M. On the Emissivity of π^0-Decay Gamma Radiation in the Vicinity of Accelerators of Galactic Cosmic Rays. *Astron. Astrophys.* **1996**, *309*, 917–928.
17. Acharya, B.S.; Agudo, I.; Samarai, I.A.; et al. *Science with the Cherenkov Telescope Array*; World Scientific Publishing: Singapore, 2018.
18. Aartsen, M.G.; Abbasi, R.; Ackermann, M.; et al. IceCube-Gen2: The Window to the Extreme Universe. *J. Phys. G* **2021**, *48*, 060501.
19. Adrian-Martinez, S.; Ageron, M.; Aharonian, F.; et al. Letter of Intent for KM3NeT 2.0. *J. Phys. G* **2016**, *43*, 084001.
20. Huentemeyer, P.; BenZvi, S.; Dingus, B.; et al. The Southern Wide-Field Gamma-Ray Observatory (SWGO): A Next-Generation Ground-Based Survey Instrument. *Bull. Am. Astron. Soc.*, 2019; *51*, 109.
21. Lopez-Coto, R.; Mitchell, A.; Angüner, E.O.; et al. Galactic Science with the Southern Wide-Field Gamma-Ray Observatory. *PoS* **2022**, *ICRC2021*, 892.
22. Abreu, P.; Alfaro, R.; Alfonso, A.; et al. Science Prospects for the Southern Wide-Field Gamma-Ray Observatory: SWGO **2025**, arXiv:2506.01786.
23. Bolatto, A.D.; Wolfire, M.; Leroy, A.K. The CO-to-H_2 Conversion Factor. *Annu. Rev. Astron. Astrophys.* **2013**, *51*, 207–268.

24. Kelner, S.R.; Aharonian, F.A.; Bugayov, V.V. Energy Spectra of Gamma Rays, Electrons, and Neutrinos Produced at Proton-Proton Interactions in the Very High Energy Regime. *Phys. Rev. D* **2006**, *74*, 034018.
25. Kafexhiu, E.; Aharonian, F.; Taylor, A.M.; et al. Parametrization of Gamma-Ray Production Cross Sections for *pp* Interactions in a Broad Proton Energy Range from the Kinematic Threshold to PeV Energies. *Phys. Rev. D* **2014**, *90*, 123014.
26. Tan, L.C.; Ng, L.K. Calculation of the Equilibrium Antiproton Spectrum. *J. Phys. G* **1983**, *9*, 227.
27. Ackermann, M.; Ajello, M.; Allafort, A.; et al. Detection of the Characteristic Pion-Decay Signature in Supernova Remnants. *Science* **2013**, *339*, 807.
28. Gabici, S.; Aharonian, F.A.; Blasi, P. Gamma Rays from Molecular Clouds. *Astrophys. Space Sci.* **2007**, *309*, 365–371.
29. Strong, A.W.; Moskalenko, I.V.; Ptuskin, V.S. Cosmic-Ray Propagation and Interactions in the Galaxy. *Annu. Rev. Nucl. Part. Sci.* **2007**, *57*, 285–327.
30. Pazianotto, M.T.; Pilling, S.; Molina, J.M.Q.; et al. Energy Deposition by Cosmic Rays in the Molecular Cloud Using GEANT4 Code and Voyager I Data. *Astrophys. J.* **2021**, *911*, 129.
31. Aharonian, F.A. *Very High Energy Cosmic Gamma Radiation: A Crucial Window on the Extreme Universe*; World Scientific Publishing: Singapore, 2004.
32. Padovani, M.; Ivlev, A.V.; Galli, D.; et al. Impact of Low-Energy Cosmic Rays on Star Formation. *Space Sci. Rev.* **2020**, *216*, 29.
33. Gabici, S. Cosmic Rays and Molecular Clouds. In *Cosmic Rays in Star-Forming Environments*; Torres, D.F., Reimer, O., Eds.; Springer: Cham, Switzerland, 2013; Volume 34, p. 221.
34. Mori, M. Nuclear Enhancement Factor in Calculation of Galactic Diffuse Gamma-Rays: A New Estimate with DPMJET-3. *Astropart. Phys.* **2009**, *31*, 341–343.
35. Ginzburg, V.L.; Syrovatskii, S.I. *The Origin of Cosmic Rays*; Pergamon Press: Oxford, UK, 1964.
36. Skilling, J. Cosmic Ray Streaming—I. Effect of Alfvén Waves on Particles. *Mon. Not. R. Astron. Soc.* **1975**, *172*, 557–566.
37. Kulsrud, R.; Pearce, W.P. The Effect of Wave-Particle Interactions on the Propagation of Cosmic Rays. *Astrophys. J.* **1969**, *156*, 445.
38. Nava, L.; Gabici, S. Anisotropic Cosmic Ray Diffusion and Gamma-Ray Production Close to Supernova Remnants, with an Application to W28. *Mon. Not. R. Astron. Soc.* **2013**, *429*, 1643–1651.
39. Gabici, S.; Aharonian, F.A. Searching for Galactic Cosmic-Ray Pevatrons with Multi-TeV Gamma Rays and Neutrinos. *Astrophys. J. Lett.* **2007**, *665*, L131–L134.
40. Padovani, M.; Galli, D.; Glassgold, A.E. Cosmic-Ray Ionization of Molecular Clouds. *Astron. Astrophys.* **2009**, *501*, 619–631.
41. Indriolo, N.; McCall, B.J. Investigating the Cosmic-Ray Ionization Rate in the Galactic Diffuse Interstellar Medium through Observations of H_3^+. *Astrophys. J.* **2012**, *745*, 91.
42. Tatischeff, V.; Decourchelle, A.; Maurin, G. Nonthermal X-Rays from Low-Energy Cosmic Rays: Application to the 6.4 keV Line Emission from the Arches Cluster Region. *Astron. Astrophys.* **2012**, *546*, A88.
43. Abdo, A.A.; Ackermann, M.; Ajello, M.; et al. Observation of Supernova Remnant IC443 with the Fermi Large Area Telescope. *Astrophys. J.* **2010**, *712*, 459–468.
44. Abdo, A.A.; Ackermann, M.; Ajello, M.; et al. Gamma-Ray Emission from the Shell of Supernova Remnant W44 Revealed by the Fermi LAT. *Science* **2009**, *327*, 1103–1106.
45. Casanova, S.; Aharonian, F.A.; Fukui, Y.; et al. Molecular Clouds as Cosmic-Ray Barometers. *Publ. Astron. Soc. Jpn.* **2010**, *62*, 769.
46. Ackermann, M.; Ajello, M.; Allafort, A.; et al. Fermi Large Area Telescope Study of Cosmic Rays and the Interstellar Medium in Nearby Molecular Clouds. *Astrophys. J.* **2012**, *755*, 22.
47. Aharonian, F.; Peron, G.; Yang, R.; et al. Probing the Sea of Galactic Cosmic Rays with Fermi-LAT. *Phys. Rev. D* **2020**, *101*, 083018.
48. Abdo, A.A.; Ackermann, M.; Ajello, M.; et al. Fermi Observations of Cassiopeia and Cepheus: Diffuse Gamma-Ray Emission in the Outer Galaxy. *Astrophys. J.* **2010**, *710*, 133–149.
49. Yang, R.Z.; de Oña Wilhelmi, E.; Aharonian, F. Probing Cosmic Rays in Nearby Giant Molecular Clouds with the Fermi Large Area Telescope. *Astron. Astrophys.* **2014**, *566*, A142.
50. Aharonian, F. Discovery of Very High Energy Gamma-Ray Emission Coincident with Molecular Clouds in the W28 (G6.4-0.1) Field. *Astron. Astrophys.* **2008**, *481*, 401.
51. Acciari, V.A.; Aliu, E.; Arlen, T.; et al. Observation of Extended Very High Energy Emission from the Supernova Remnant IC 443 with VERITAS. *Astrophys. J. Lett.* **2009**, *698*, L133–L137.
52. Abdo, A.A.; Ackermann, M.; Ajello, M.; et al. Fermi LAT Discovery of Extended Gamma-Ray Emission in the Direction of Supernova Remnant W51C. *Astrophys. J. Lett.* **2009**, *706*, L1–L6.
53. Jogler, T.; Funk, S. Revealing W51C as a Cosmic Ray Source Using Fermi-LAT Data. *Astrophys. J.* **2016**, *816*, 100.
54. Cao, Z.; Aharonian, F.; An Q.; et al. Measurement of Ultra-High-Energy Diffuse Gamma-Ray Emission of the Galactic Plane from 10 TeV to 1 PeV with LHAASO-KM2A. *Phys. Rev. Lett.* **2023**, *131*, 151001.

55. Fang, K.; Murase, K. Multimessenger Implications of Sub-PeV Diffuse Galactic Gamma-Ray Emission. *Astrophys. J.* **2021**, *919*, 93.
56. Ackermann, M.; Ajello, M.; Atwood, W.B.; et al. Fermi-LAT Observations of the Diffuse γ-Ray Emission: Implications for Cosmic Rays and the Interstellar Medium. *Astrophys. J.* **2012**, *750*, 3.
57. Gaggero, D.; Grasso, D.; Marinelli, A.; et al. The Gamma-Ray and Neutrino Sky: A Consistent Picture of Fermi-LAT, Milagro, and IceCube Results. *Astrophys. J. Lett.* **2015**, *815*, L25.
58. Evoli, C.; Gaggero, D.; Vittino, A.; et al. Cosmic-Ray Propagation with DRAGON2: I. Numerical Solver and Astrophysical Ingredients. *J. Cosmol. Astropart. Phys.* **2017**, *02*, 015.
59. Amenomori, M.; Bao, Y.W.; Bi, X.J.; et al. First Detection of Sub-PeV Diffuse Gamma Rays from the Galactic Disk: Evidence for Ubiquitous Galactic Cosmic Rays beyond PeV Energies. *Phys. Rev. Lett.* **2021**, *126*, 141101.
60. Sandrock, A. Searches for Galactic Neutrinos with the IceCube Neutrino Observatory. In Proceedings of the 58th Rencontres de Moriond on Very High Energy Phenomena in the Universe, La Thuile, Italy, 24–31 March 2024.
61. Strong, A.W.; Moskalenko, I.V. Propagation of Cosmic-Ray Nucleons in the Galaxy. *Astrophys. J.* **1998**, *509*, 212–228.
62. Porter, T.A.; Jóhannesson, G.; Moskalenko, I.V. The GALPROP Cosmic-Ray Propagation and Nonthermal Emissions Framework: Release v57. *Astrophys. J. Suppl.* **2022**, *262*, 30.
63. Schwefer, G.; Mertsch, P.; Wiebusch, C. Diffuse Emission of Galactic High-Energy Neutrinos from a Global Fit of Cosmic Rays. *Astrophys. J.* **2023**, *949*, 16.
64. Aharonian, F.; Yang, R.; de Oña Wilhelmi, E. Massive Stars as Major Factories of Galactic Cosmic Rays. *Nat. Astron.* **2019**, *3*, 561–567.
65. Morlino, G.; Blasi, P.; Peretti, E.; et al. Particle Acceleration in Winds of Star Clusters. *Mon. Not. R. Astron. Soc.* **2021**, *504*, 6096–6105.
66. Ishihara, A. The Next Generation Neutrino Telescope: IceCube-Gen2. In Proceedings of the 38th International Cosmic Ray Conference (ICRC2023), Nagoya, Japan, 26 July–3 August 2023.
67. Aiello, S.; Albert, A.; Alshamsi, M.; et al. Astronomy Potential of KM3NeT/ARCA. *Eur. Phys. J. C* **2024**, *84*, 885.
68. Abbasi, R.; Ackermann, M.; Adams, J.; et al. Search for Extended Sources of Neutrino Emission in the Galactic Plane with IceCube. *Astrophys. J.* **2023**, *956*, 20.
69. Ackermann, M.; Ajello, M.; Allafort, A.; et al. A Cocoon of Freshly Accelerated Cosmic Rays Detected by Fermi in the Cygnus Superbubble. *Science* **2011**, *334*, 1103–1107.
70. Bartoli, B.; Bernardini, P.; Bi, X.J.; et al. Identification of the TeV Gamma-Ray Source ARGO J2031+4157 with the Cygnus Cocoon. *Astrophys. J.* **2014**, *790*, 152.
71. Abeysekara, A.U.; Albert, A.; Alfaro, R.; et al. Multiple Galactic Sources with Emission Above 56 TeV Detected by HAWC. *Phys. Rev. Lett.* **2020**, *124*, 021102.
72. LHAASO Collaboration. An Ultrahigh-Energy γ-Ray Bubble Powered by a Super PeVatron. *Sci. Bull.* **2024**, *69*, 449–457.
73. Abbasi, R.; Ackermann, M.; Adams, J.; et al. The IceCube-Gen2 Collaboration—Contributions to the 37th International Cosmic Ray Conference (ICRC2021). arXiv **2021**, arXiv:2107.06968.
74. Aiello, S.; Akrame, S.E.; Ameli, F.; et al. Sensitivity of the KM3NeT/ARCA Neutrino Telescope to Point-Like Neutrino Sources. *Astropart. Phys.* **2019**, *111*, 100–110.
75. Aynutdinov, V.M.; Allakhverdyan, V.A.; Avrorin, A.D.; et al. Large Neutrino Telescope Baikal-GVD: Recent Status. *PoS* **2023**, *ICRC2023*, 976.
76. Allakhverdyan, V.A.; Avrorin, A.D.; Avrorin, A.V.; et al. Diffuse Neutrino Flux Measurements with the Baikal-GVD Neutrino Telescope. *Phys. Rev. D* **2023**, *107*, 042005.
77. Ginsburg, A. A Review of the W51 Cloud. *arXiv* **2017**, arXiv:1702.06627.
78. Aleksić, J.; Álvarez, E.A.; Antonelli, L.A.; et al. Morphological and Spectral Properties of the W51 Region Measured with the MAGIC Telescopes. *Astron. Astrophys.* **2012**, *541*, A13.
79. Koo, B.C.; Moon, D.S. Interaction between the W51C Supernova Remnant and a Molecular Cloud. I. H I 21 Centimeter Line Observations. *Astrophys. J.* **1997**, *475*, 194–210.
80. Brogan, C.L.; Goss, W.M.; Hunter, T.R.; et al. OH (1720 MHz) Masers: A Multiwavelength Study of the Interaction between the W51C Supernova Remnant and the W51B Star Forming Region. *Astrophys. J.* **2013**, *771*, 91.
81. Schneider, N.; Bontemps, S.; Simon, R.; et al. A New View of the Cygnus X Region. KOSMA ^{13}CO 2 to 1, 3 to 2, and ^{12}CO 3 to 2 Imaging. *Astron. Astrophys.* **2006**, *458*, 855–871.
82. Rygl, K.L.J.; Brunthaler, A.; Sanna, A.; et al. Parallaxes and Proper Motions of Interstellar Masers toward the Cygnus X Star-Forming Complex. I. Membership of the Cygnus X Region. *Astron. Astrophys.* **2012**, *539*, A79.
83. Wright, N.J.; Drew, J.E.; Mohr-Smith, M. The Massive Star Population of Cygnus OB2. *Mon. Not. R. Astron. Soc.* **2015**, *449*, 741–760.
84. Li, W.; Huang, T.Q.; Xu, D.; et al. Search for Neutrino Emission from the Cygnus Bubble Based on LHAASO γ-Ray Observations. *Astrophys. J.* **2024**, *969*, 6.
85. Morris, M.; Serabyn, E. The Galactic Center Environment. *Annu. Rev. Astron. Astrophys.* **1996**, *34*, 645–702.
86. Ferriere, K.; Gillard, W.; Jean, P. Spatial Distribution of Interstellar Gas in the Innermost 3 kpc of Our Galaxy. *Astron.*

Astrophys. **2007**, *467*, 611–627.

87. Abramowski, A.; Aharonian, F.; Benkhali, F.A.; et al. Acceleration of Petaelectronvolt Protons in the Galactic Centre. *Nature* **2016**, *531*, 476.
88. Scherer, A.; Cuadra, J. Multiwavelength Galactic Center Gamma-Ray Observations Explained by a Unified Cosmic-Ray Dynamics Model. *Astron. Astrophys.* **2024**, *690*, L14.
89. Celli, S.; Palladino, A.; Vissani, F. Neutrinos and γ-Rays from the Galactic Center Region after H.E.S.S. Multi-TeV Measurements. *Eur. Phys. J. C* **2017**, *77*, 66.
90. Gabici, S.; Casanova, S.; Aharonian, F.A.; et al. Constraints on the Cosmic Ray Diffusion Coefficient in the W28 Region from Gamma-Ray Observations. In Proceedings of the Annual Meeting of the French Society of Astronomy and Astrophysics, Marseille, France, 21–24 June 2010; p. 3131.
91. Sunny, A.; Cardillo, M.; Tutone, A. Studying SNR-MC Interactions as Galactic PeVatrons in the Era of CTAO and ASTRI Mini-Array. *PoS* **2025**, *ICRC2025*, 853.
92. Pedaletti, G.; Torres, D.F.; Gabici, S.; et al. CTA and Cosmic-Ray Diffusion in Molecular Clouds. *AIP Conf. Proc.* **2012**, *1505*, 797–800.
93. Dubos, C.; Sharma, P.; Patel, S.; Suomijärvi, T. Cherenkov Telescope Array Observatory Sensitivity to Heavy Galactic Cosmic Rays and the Shape of Particle Spectrum. *J. Cosmol. Astropart. Phys.* **2025**, *02*, 078.
94. Schroeder, F.G. Science Potential and Technical Design of the IceCube-Gen2 Surface Array. *arXiv* **2024**, arXiv:2502.19950.
95. Abbasi, R.; Ackermann, M.; Adams, J.; et al. Searches for Neutrinos from Large High Altitude Air Shower Observatory Ultra-High-Energy γ-Ray Sources Using the IceCube Neutrino Observatory. *Astrophys. J. Lett.* **2023**, *945*, L8.
96. Abe, S.; Abhir, J.; Abhishek, A.; et al. Prospects for a Survey of the Galactic Plane with the Cherenkov Telescope Array. *J. Cosmol. Astropart. Phys.* **2024**, *10*, 081.
97. Schwefer, G. Dissecting the Diffuse Gamma-Ray Emission of the Galaxy with the HAWC Observatory. *arXiv* **2025**, arXiv:2509.03189.
98. Aab, A.; Abreu, P.; Aglietta, M.; et al. The Pierre Auger Observatory Upgrade - Preliminary Design Report. *arXiv* **2016**, arXiv:1604.03637.
99. Selina, R.J.; Murphy, E.J.; McKinnon, M.; et al. The Next-Generation Very Large Array: A Technical Overview. In Proceedings of the Ground-Based and Airborne Telescopes VII, Austin, TX, USA, 10–15 June 2018.
100. Peron, G.; Aharonian, F. Probing the Galactic Cosmic-Ray Density with Current and Future γ-Ray Instruments. *Astron. Astrophys.* **2022**, *659*, A57.
101. Peron, G.; Aharonian, F.; Casanova, S.; et al. Probing the Cosmic-Ray Density in the Inner Galaxy. *Astrophys. J. Lett.* **2021**, *907*, L11.